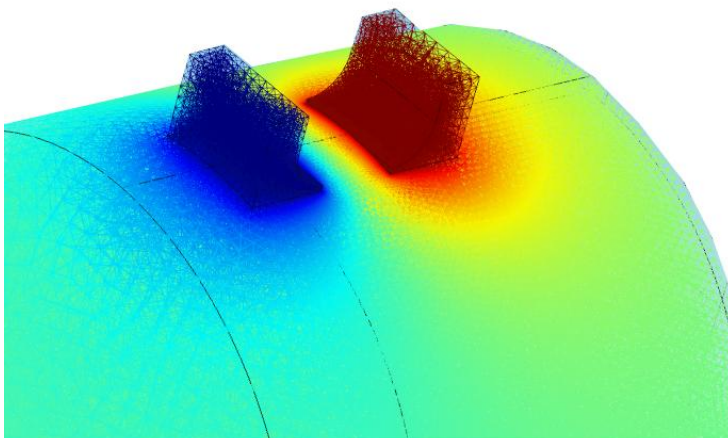
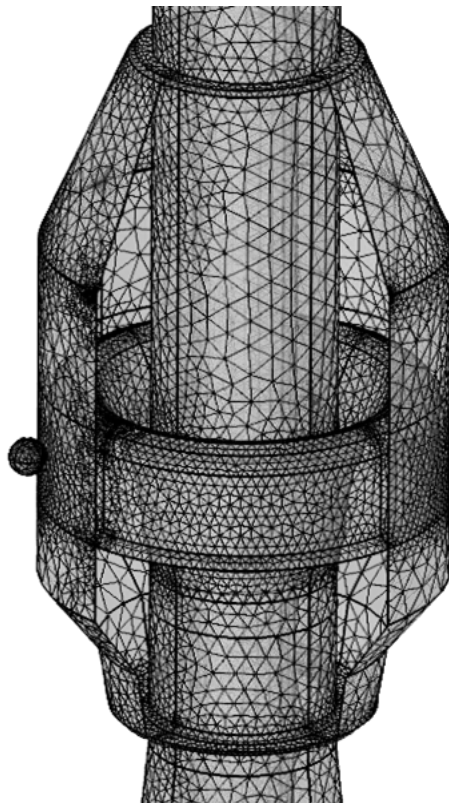


# Investigation on termination oil-rubber interface parallel to electric field with water contamination

H.Di





# Investigation on termination oil-rubber interface parallel to electric field with water contamination

By

Hong Di

in partial fulfilment of the requirements for the degree of

**Master of Science**

in Electrical Engineering - Electrical Sustainable Energy

at the Delft University of Technology,

to be defended publicly on Friday August 18<sup>th</sup>, 2017 at 13:00

Student number:	4502701	
Supervisors:	Dr. Armando Rodrigo Mor Dr. ir. Alex Tsekmes	
Thesis committee:	Prof. dr. ir.P.T.M.Vaessen Dr. ir. Armando Rodrigo Mor Dr. ir. Milos Cvetkovic Dr. ir. Alex Tsekmes	TU Delft TU Delft TU Delft Prysmian Group



**Prysmian**  
Group

The work in this thesis was supported by *Prysmian Group Netherlands B.V.* Their cooperation is hereby gratefully acknowledged.

# Acknowledgement

This master thesis work was strongly supported by Prysmian Group Netherlands B.V. and the department of Electrical Sustainable Energy of TU Delft.

Firstly, I want to express my thankfulness and appreciation to my supervisors and mentors, Armando, Alex, and Riccardo. There is no doubt that this work cannot be done without your generous help. The suggestions you gave, no matter relating to my study or life, always inspire me a lot. I'm glad to meet you at the other part of this planet.

Furthermore, it's a great honor to work as a member of Prysmian Group Netherlands B.V. and a student in the department of Electrical Sustainable Energy of TU Delft. I am deeply impressed by these two leading organizations and the people there. Thanks to my lab supervisors, Paul, Radek, Remko, Wim, and to my nice colleagues in Prysmian, especially Panos!

I want say thank you to my family as well. Their son is proud of his family.

In the end, I have to say thank you to this country, the Netherlands. This is a wonderful place with awesome people. The experience I had here is priceless.

Best wishes to all of you, sincerely.

## Abstract

At the end of a power transmission line, the cable should be terminated carefully, otherwise it will create problems during the operation. A special equipment called termination is designed to tackle down the problems from cable ends. The main functional part of a termination is a piece of rubber with a cone shape. This rubber cone has a semi-conductive layer which is connected with ground potential. By doing this, the cone smoothens the concentric equipotential lines at the cable end, so the electric field stress there can be decreased. The cone in the termination is called stress cone. However, insulation degradation on the termination stress cone due to water contamination is often found in its operation. This, in the end, will cause operation failures in the power network. This research aims to investigate the influences brought by water contamination on the stress cone, and discuss possibilities of detecting the presence of water content by using electrical methods. By using 3D FEM simulations, the changes of electric field distribution, especially the field along the oil-rubber interface, were studied. Based on the simulation results, we built up a small scale test setup to observe how water contamination behaves on the oil-rubber interface, and measured the changes of partial discharge signals and  $\tan\delta$  values. As conclusions, we discussed the electrical ways of detecting the presence of water contamination on the stress cone, and gave suggestions for the future work.

# Contents

1	Introduction.....	7
1.1.	Modern power transmission system.....	7
1.2.	Solutions of the cable end .....	7
1.3.	Challenges from the water contamination.....	8
1.4.	Previous research on this topic.....	8
1.5.	Objectives of the thesis.....	9
	➤ Electric field change due to the presence of water contamination on the oil-rubber interface.....	9
	➤ Small scale test setup construction for measurement and observation on the oil-rubber interface.....	9
	➤ Conclusions of thesis work and recommendations for future work.....	9
1.6.	Outline of this thesis report.....	10
2	Electric field analysis on the termination.....	11
2.1.	Insulating material properties and E-field.....	11
	➤ Insulating properties of solid material .....	11
	➤ Insulating properties of liquid material .....	11
	➤ Insulating properties of the interface and triple point .....	11
	➤ The importance of the E-field .....	12
	➤ Water contamination in terminations .....	12
2.2.	2D model and the simulation by FEM .....	13
2.3.	Electric field analysis on the termination without water contamination .....	14
2.4.	The need of a 3D model for simulation when water droplets present.....	16
	➤ 3D model simulation results .....	17
2.5.	Electrostatic study on the effect brought by the water droplets .....	17
	➤ The effect caused by different positions of water droplet.....	19
	➤ The effect caused by the amount of water droplets .....	20
	➤ The effect caused by the sizes of water droplets.....	21
	➤ The effect caused by the relative permittivity of water droplets .....	22
2.6.	Electric current study on the effect brought by the water droplets.....	23
	➤ The electric field for water droplets with different conductivities under 50Hz .....	24
	➤ The electric field of water droplet under different frequency(0.5 S/m) .....	26
2.7.	Theoretical highest electric field situation.....	26
2.8.	Conclusion from the simulation results .....	29
	➤ The influential parameters .....	29
	➤ Field enhancement due to water contamination.....	29

3	Small scale test setup design .....	30
3.1.	The objectives of the small scale test .....	30
3.2.	Test setup design by 3D simulation .....	30
3.3.	Real test setup construction.....	33
	➤ Testing area description .....	34
	➤ Measuring area .....	35
4	Partial discharge measurement.....	37
4.1.	PD detector explanations and detecting circuit.....	37
4.2.	PD sources in the test setup .....	38
4.3.	PD on the oil-rubber interface.....	41
4.4.	PD on the oil-rubber interface with water droplets.....	41
	➤ Experiments with big size water droplets.....	41
	➤ Experiments with small size water droplets.....	43
4.5.	Tests on the oil-rubber interface with oil-water emulsion .....	45
	➤ Preparation of water-oil emulsion samples .....	45
	➤ PD measurement with water-oil emulsion .....	46
4.6.	PD measurement on long term process .....	48
5	Tan $\delta$ measurement.....	53
6	Conclusions & Recommendations .....	58
6.1.	Conclusions .....	58
	➤ Electric field distributions on the stress cone surface with water contamination.....	58
	➤ Water content detecting by PD measurement.....	58
	➤ Water content detecting by tan $\delta$ measurement .....	58
6.2.	Recommendations.....	58
	➤ Test setup design on long term experiment.....	58
	➤ Investigations on triple points in the oil termination.....	59
	➤ PD sensor design and installations.....	59
	➤ Development of non-electrical detections .....	59

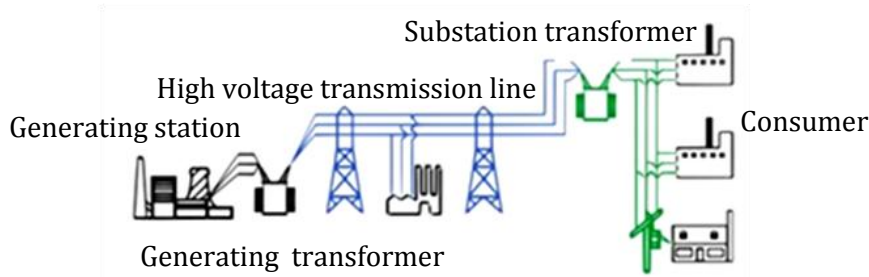
## List of figures

Figure 1 Electrical power network.....	7
Figure 2 Cable system illustration .....	7
Figure 3 Cable-end controlling.....	7
Figure 4 Oil termination and inside cone.....	8
Figure 5 Electrical faults in the oil termination due to water contamination [4]. .....	8
Figure 6 Illustration of the interface in a termination.....	11
Figure 7 illustration of the triple point in a termination: the blue line indicates the triple point where oil, XLPE and rubber converge .....	12
Figure 8 Termination model built in AutoCAD; meshing results in COMSOL.....	13
Figure 9 Equivalent electric circuit under static simulation.....	13
Figure 10 Electric field distribution under 0 kV with different positions of semi-conductive cone .....	15
Figure 11 Illustration of the Arc length and electric field composition on perpendicular and parallel direction under 70 kV.....	15
Figure 12 Electric field decompositions along the oil-rubber interface: amplitude; perpendicular; parallel.....	15
Figure 13 Example of water droplet in a 2D model and a 3D model.....	16
Figure 14 Electric field amplitude distribution under 70 kV from 3D model simulation.....	17
Figure 15 Electric field amplitude distribution under 70 kV with a droplet presenting on the cone surface.....	17
Figure 16 Equipotential line distribution, without and with water droplet under 70 kV.....	18
Figure 17 Equipotential lines go through different materials with different relative permittivity .....	18
Figure 18 Equipotential line distribution under 70 kV with droplet placed at different positions .....	19
Figure 19 Equipotential line distribution under 70 kV with different number of droplets.....	20
Figure 20 Equipotential line distribution under 70 kV with different sizes of droplets .....	21
Figure 21 Equipotential lines distribution under 70 kV with droplets having different relative permittivity.....	22
Figure 22 The horizontal cross section of the termination .....	23
Figure 23 Equivalent electric circuits under electric static study and frequency domain study .	23
Figure 24 Potential lines distribution under 70 kV for water droplets with different conductivities .....	24
Figure 25 Scenario which produces the highest electric field strength under 70 kV.....	27
Figure 26 Electric field at one line of the stress cone under 70 kV .....	27
Figure 27 Electric field amplitude along the stress cone under 70 kV .....	27
Figure 28 Electric field amplitude along the line for W Y Z direction under 70 kV.....	28
Figure 29 Highest electric field amplitude composition on perpendicular and parallel directions under 70 kV .....	28
Figure 30 Small scale test setup sample.....	30
Figure 31 Simulation result of preliminary test setup under 30 kV .....	31
Figure 32 Electric field distribution under 30 kV with boot shape electrodes .....	32
Figure 33 Size of the cone; electrode shape; final set up` .....	32
Figure 34 The electric potential distribution and the electric field distribution of our test setup under 30 kV .....	32
Figure 35 Testing area configuration .....	33
Figure 36 The components in the testing area .....	34
Figure 37 The main testing subject in the oil aquarium .....	34
Figure 38 The logic of test setup designing.....	35
Figure 39 Scheme of testing area and measuring area.....	35

Figure 40 The measuring area.....	36
Figure 41 connection between the PD receiver and the computer.....	36
Figure 42 Partial discharge detection circuit illustration .....	37
Figure 43 Main operation window of the PD detector .....	37
Figure 44 Different visualizations of the PD.....	38
Figure 45 Toroid cap on the top of the conducting bar.....	39
Figure 46 The partial discharge gone after putting insulating tubes.....	40
Figure 47 The electrode before and after the modification .....	40
Figure 48 Syringe used for injecting water droplet.....	41
Figure 49 1ml syringe .....	43
Figure 50 The water droplet eventually becomes like a thin layer of cotton .....	44
Figure 51 PD signal for single water droplet at 45 kV.....	44
Figure 52 Prepared water-oil emulsion samples before getting heat up .....	45
Figure 53 The oven for heating up the water-oil emulsion cans.....	46
Figure 54 The examples of resulted water-oil emulsion .....	46
Figure 55 The water-oil emulsion layer on the stress cone surface .....	46
Figure 56 The partial discharge pattern and classification map in water-oil emulsion experiments.....	47
Figure 57 Complex plane of the losses in dielectric; Parallel equivalent circuit .....	53
Figure 58 $\tan\delta$ measurement device and voltage amplifier.....	53
Figure 59 The IDAX impedance measuring circuit .....	54
Figure 60 Measuring circuit for the $\tan\delta$ .....	54
Figure 61 Teflon ring for isolating the conducting bar and grounding lead .....	55
Figure 62 $\tan\delta$ on stress cone with water contamination after putting Teflon ring; three terminal circuit.....	56
Figure 63 Dedicated $\tan\delta$ measuring device and detecting circuit.....	56
Figure 64 $\tan\delta$ of pure oil(line below) and water-oil emulsion(line above).....	57

# 1 Introduction

## 1.1. Modern power transmission system



*Figure 1 Electrical power network*

The electrical power consumed by customers is generated by power generating stations. In between the generating stations and consumer sites, there is a complete network for transmitting power [1]. This transmission network is also called cable system which consists of power cables and all kinds of accessories. Typically, there are three main parts in a cable system, these are cables, cable joints and terminations .

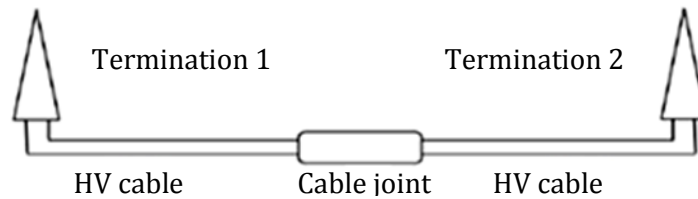


*Figure 2 Cable system illustration*

Just like vessels transporting blood in human bodies, power cables are used to carry and transmit electrical power. Due to the restrictions of manufacturing and limitations of shipping, power cables cannot be produced over certain length. Therefore, joints are made to link two segments of cables together. At the end of a power transmission line, the cable should be terminated carefully, otherwise it will create problems during the operation [2].

## 1.2. Solutions of the cable end

A special equipment called termination is designed to tackle down the problem from cable end. The main functional part of a termination is a piece of rubber with cone shape. This rubber cone has a semi-conductive layer which is connected with ground potential.

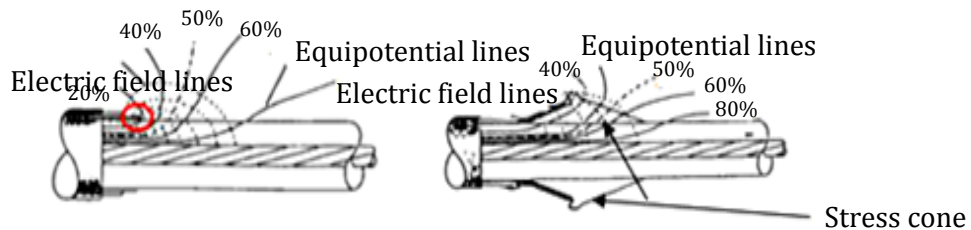


*Figure 3 Cable-end controlling*

By doing this, the cone smoothens the concentric equipotential lines at the cable end, therefore the electric field stress there can be decreased. That's why this rubber cone is also called stress cone. The stress cone cannot work independently. It should be put in a container or a housing which isolates the cone from outside. The space between the stress cone and the housing wall is normally filled with insulating material to provide enough dielectric strength. Oil type material is widely chosen as the housing insulating material, since it not only has outstanding insulating performance but can also effectively transfer and cool down the heat generated by the inner components. The whole setup here is called oil cable termination. This type of terminations has been used in power industry for decades. However, it doesn't mean that the oil termination is flawless. Impurities, especially water contamination, in the insulating oil will create a lot of troubles during its operation.



*Figure 4 Oil termination and inside cone*

### 1.3. Challenges from the water contamination

Water contamination is regarded as the major cause for oil-filled termination failures [3]. Water content could ingress into the termination housing through top bolt due to poor tightening techniques during sealing process when it is manufactured. And during its operating life, water ingress could also from ambient environment [4]. This ingress of water content will contaminate the insulating oil. Normally there is only a small amount of water in an oil termination. And water content is always dissolved in the oil as long as its amount is below the solubility of oil. The solubility is decided by the type of the oil and is mainly influenced by ambient temperature [5]. So in real situation, water contamination could be both dissolved water content, which is also known as oil-water emulsion, and liquid water content, such as water droplet on the stress cone surface. Based on the investigation [4], different kinds of termination faults happened due to water contamination. These faults include regional breakdown, surface treeing and material erosion. Water content in the oil termination could also cause regional overheating which accelerates material degradation[6].



*Figure 5 Electrical faults in the oil termination due to water contamination [4].*

### 1.4. Previous research on this topic

In order to investigate the effect from water contamination in the oil termination, Prysmian Netherlands carried out a project with Technical University of Delft in 2016. In that project [7]: a 2D model of the termination was built and its electric field was simulated; the breakdown strength of termination oil, dielectric response and partial discharge activity in different oil

samples were tested. However a 2D model is not enough to simulate the effects brought by water contamination. Secondly there was no intention on the oil-rubber interface where most of the faults happened. Moreover, short term PD measurement is not convincing to adopt this method for onsite detection. Experiment with a longer period is required to valid the effectiveness of the PD detecting method.

Besides the former research, there are some other research related to the our topic. In the research [4], oil termination failure due to water contamination ingression was reviewed, and a particular moisture sensor was evaluated. The process of static charges accumulation on the liquid-solid interface was recognized by [8].The discharge propagating along the liquid- solid interface was investigated by [9]. The surface degradation of solid material caused by oil-water emulsion was researched by [3].

The studies mentioned above can be used as instructions for our own research. The objectives of this thesis work can be found below.

### 1.5. Objectives of the thesis

Our thesis objectives are based on the requests from Prysmian and taking into account the suggestions from previous works.

#### ➤ **Electric field change due to the presence of water contamination on the oil-rubber interface**

First we would like to know the electric field change due to the presence of water contamination on the oil-rubber interface. The change of the electric field includes both the amplitude and the directions. From our point of view, it is highly important to know the amplitude change in the parallel direction with the oil-rubber interface. The change may correlate with the parameters of water contamination. These parameters may include the size of the contamination, the relative permittivity or the electrical conductivity of the moisture, etc. This part can be done by using a 3D model of the termination and simulating on the electric field distribution.

#### ➤ **Small scale test setup construction for measurement and observation on the oil-rubber interface**

Later on we need to build up a small scale test setup and observe the change on the oil-rubber interface with water contamination under electric stress. It's not easy to observe the phenomena in an operating cable termination, since the out layer is not transparent and it is dangerous to get close to high voltage equipment. By building up a small scale test setup, we could replicate the situation in a more controllable and observable way. In order to get valid data, we have to come up with a proper configuration for our setup. Relevant components should use the same material from a real termination.

#### ➤ **Conclusions of thesis work and recommendations for future work**

In the end, we would like to discuss the possibility of detecting the water contamination in the termination and propose for future work. By designing and conducting series of high voltage experiments, measuring results can be used as an indication of the presence of water contamination. After scientific analyses, we can give conclusions on the possibility of detecting the water content in the termination and propose for future work.

## 1.6. Outline of this thesis report

The first part of this report is an introduction to our research. Following with chapter 2 where we discuss the electrical simulations performed on the termination 3D models. In chapter 3 the process of building up a small scale test setup is presented. Electrical measurements are elaborated in chapter 4 and 5. In the last chapter, we discuss the possibilities of detecting the water contamination, and propose for future work.

## 2 Electric field analysis on the termination

### 2.1. Insulating material properties and E-field

The main insulating material in the termination includes XLPE, rubber and oil. For different material, they have different aging process and breakdown mechanism.

#### ➤ Insulating properties of solid material

Normally the solid material is chosen to be the insulating material due to its self-supporting structure and high breakdown strength. For example, XLPE, also known as cross-linked polyethylene, is widely used as cable insulation. Some investigations have been done concerning about the aging state of the XLPE insulation. By testing the oxygen induction time or measuring the crystallinity of the XLPE, the aging state can be decided [10]. There is also research focusing on the activation energy and the isothermal relaxation current of the XLPE [11]. These methods are based on the fact that the XLPE is semi-crystalline polymer, so the electrical performance of it depends on its C-O elements and polymer structure.

Rubber is another commonly used insulating material, such as the stress cone in the termination. It's not only the dielectric strength but also the elasticity of the rubber make it suitable for functioning as the cable accessories. By elasticity, it means that the stress cone can be stretched to fit with the cable. By stretching, the rubber cone also provides necessary pressure on the cable and guarantees its fixation. The pressure from the rubber on the cable insulation prevents the air bubbles in between the rubber and XLPE interface. Otherwise the air bubble may cause detrimental problems to the termination. The insulating properties of the rubber is dependent on the ambient temperature [12].

The electrical degradation of the solid material is often caused by the inside cavities. This imperfection originates from the impurity during the production process.

#### ➤ Insulating properties of liquid material

Liquid insulating material, like the oil used in the termination, is also a widely adopted insulating solution. Unlike solid insulation which has permanent defects after a fault happened, liquid insulation is able to electrically self-heal. Another advantage of liquid insulation is its heat transferring ability, which makes it the best choice for transformers and cable accessories. Obviously, a container is always needed to house the liquid. The main drawback of liquid insulating material is that they are normally combustible [2].

#### ➤ Insulating properties of the interface and triple point

Besides the insulating material itself, it is also very important to discuss the insulating properties of the interface between two different materials and the triple point shared by three different

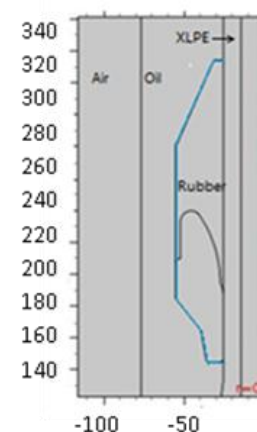


Figure 6 Illustration of the interface in a termination (size in mm)

materials. The surface of the stress cone is a typical liquid-solid interface, as it in the figure 6. The interface normally has a lower dielectric strength which results in a higher chance to cause breakdown [13]. The dielectric strength for the interface is even lower than the solid and contaminated liquid materials [14]. The interface is normally regarded as the weak part in an insulating system, since it provides a path for transporting electrons between two dielectrics. This ion collecting along the interface will result in significant tangential electric field increment and evokes surface treeing [15]. Triple point is defined as the area shared by three different dielectrics [16]. It's not necessarily to be a point. In our case, it can refer to the end of the stress cone where XLPE, rubber and oil meet together, as in the figure 7. This is not the only triple point in a termination. If there are water droplets presenting on the surface of the stress cone, the conjunction of water, oil and rubber also forms triple point. The triple point should always be given special attention in the high voltage construction, since it is always the original point of insulation degradation[17].

### ➤ The importance of the E-field

The dielectric strength of different materials has been discussed in the paragraph above. The electrical stress they bear is decided by the electric field distribution. The E-field distribution depends on the applied voltage, the configuration of the insulation system and the relative permittivity of the materials. The higher the E-field strength, the stronger the electrical stress is on the insulating materials. If the amplitude of the E-field exceeds the dielectric strength of the material, there may be partial discharge or complete breakdown in the insulation. The maximum allowed field strength along the rubber surface is 7 kV/mm, according to the company specification. Therefore, knowing the E-field distribution is of great interests for insulation system designing and testing.

### ➤ Water contamination in terminations

The presence of water contamination greatly changes the electric field distribution. And it also affects insulating properties of the components in oil terminations. The dielectric strength of termination oil will decrease when dissolving water content. Water content on the cone surface will create new interfaces and triple points. This will further decrease the dielectric strength along the stress cone surface.

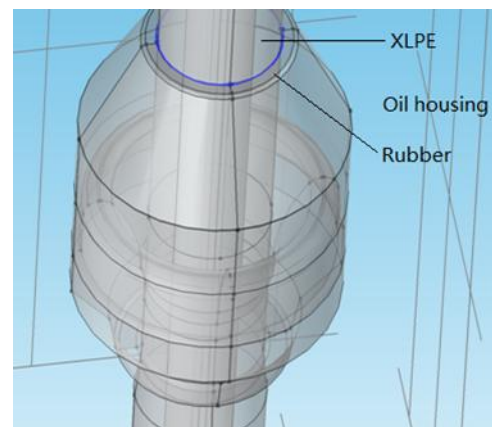


*Figure 7 illustration of the triple point in a termination: the blue line indicates the triple point where oil, XLPE and rubber converge*

### 2.2. 2D model and the simulation by FEM

In order to know the influence brought by the water content, we have to know the electric field distribution in the termination without water. The E-field calculation can be done by using finite element method, which is also known as FEM. This calculation process is also called simulation. There are several commercial soft wares for FEM calculation and the one we use here is COMSOL Multiphysics®.

First of all, a model is needed to represent our termination. It can be a 3D or 2D model depending on its geometry. Here a 2D simulation model is enough to know the E-field distribution without water content, since the termination itself is axisymmetric. As we can see from figure 6, the model contains of four main parts. They are outside air, insulating oil, rubber cone and inner cable. The model can be built either by a drawing software, like AutoCAD, or by internal drawing module from the simulation software. It's recommended to use AutoCAD if the model being built is complex, since AutoCAD has a better user interface for drawing purposes.

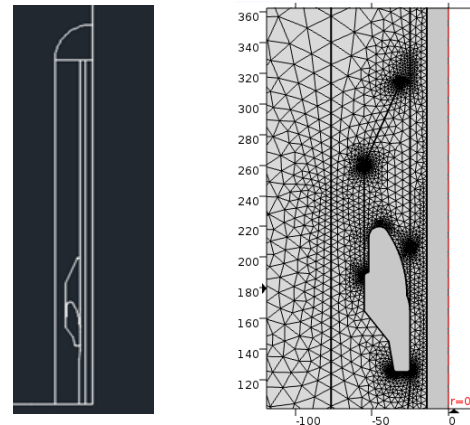


Figure 8 Termination model built in AutoCAD; meshing results in COMSOL(size in mm)

After building up the model, it can be imported to the COMSOL. The material properties of different parts in the model should be defined in order to give relevant physical properties for FEM calculation. Different physical properties are required according to the simulation types. The types of the simulation are decided by the physics involved and study modes it uses. In COMSOL, it has 11 different types of physic, such as AC/DC or Acoustic, and five study modes including Stationary or Frequency domain and etc. For us, we hope to know the electric field distribution in a termination under steady state, so a stationary study of Electrostatic type is the most suitable. For the simulation we choose, it requires the relative permittivity of different materials. This is given by the material suppliers. The values are 2.3, 3.1, 2.1, 1 for XLPE, rubber, oil and air respectively. The equivalent circuit and model configuration can be found in the figure below.

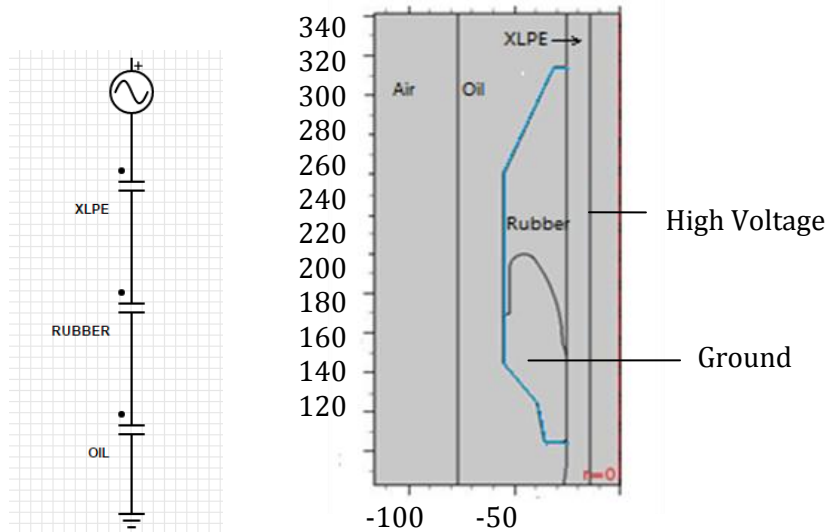


Figure 9 Equivalent electric circuit under static simulation(size in mm)

On the left part of the figure is the equivalent circuit for simulation calculation. The surface of the conductor is applied with high voltage at 70 kV. The semi-conductive rubber cone and the semi-conductive layer of the outer cable are grounded. As we can see from the circuit, the electric field distribution is capacitive if the simulation is electrostatic under stationary. The capacitance of different parts of the termination can be derived by the formula below,

$$C = \frac{2\pi L k \epsilon_0}{L_n \left[ \frac{b}{a} \right]} \quad (1)$$

This formula applies for the cylindrical structure, like terminations. In the formula, L is the length, k is the relative permittivity, The voltage distribution can be determined after yielding the capacitances.

$$V_{\text{Material}} = V_{\text{Source}} \times \frac{C_{\text{Total}}}{C_{\text{Material}}} \quad (2)$$

In the end, the electric field can be decided by the formula

$$E = \frac{dV}{dx} \quad (3)$$

After inputting in relative permittivity for each part of the termination, we need to mesh the geometry. The whole model is then meshed into pieces of triangular. For each piece of the triangular, its calculation is based on the Gauss's law and Poisson's equation.

$$\nabla \vec{D} = \rho \quad (4)$$

In which  $\rho$  is the electric charge density and D is the electric displacement or the electric flux density and is given by the constitutive relation:

$$\vec{D} = \epsilon_0 \vec{E} + \vec{P} \quad (5)$$

Where  $\epsilon_0$  is the permittivity of vacuum with value of  $8.854 \times 10^{-12}$  F/m, and  $\vec{P}$  is the electric polarization vector that describes how the material is polarized in an electric field. So  $\vec{P}$  can be seen as a function of E. Under linear condition, we get

$$\vec{D} = \epsilon_0 \epsilon_r \vec{E} \quad (6)$$

By combining the equations above,

$$-\nabla(\epsilon_0 \nabla V - \vec{P}) = \rho \quad (7)$$

The final equation is used to describe the electrostatics physics inside dielectric materials in the simulation result analysis [18].

### 2.3. Electric field analysis on the termination without water contamination

After meshing the whole geometry, the electric field distribution of a termination can be calculated. The result can be seen on the left part of the figure. Our research interests are focused on the out layer of the stress cone. From the simulation result, the point on the cone surface with the highest electric field strength is somewhere near the top of the semi-conductive cone. In order to know the reason for this position, we did other simulations where the semi-conductive cone is moved to both a lower and a higher positions.

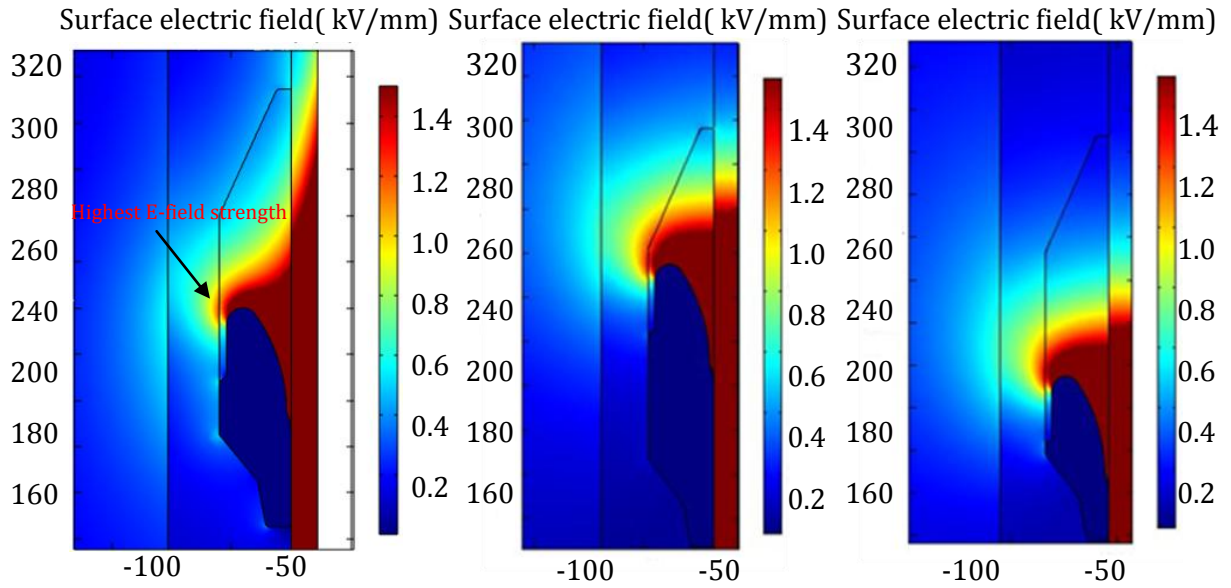


Figure 10 Electric field distribution with different positions of semi-conductive cone(size in mm)

From the figure above we can see, the position for the highest electric field is decided by the position of the semi-conductive cone. When the cone is moved up, the highest electric field point is also lifted up and vice-versa. The only information we can get from the figure is the amplitude value of the electric field strength. The electric field along the stress cone surface is of our interests as well, since the oil rubber interface is mainly affected by the electric field in parallel with it. The figure 12, 13 show the electric field strength on both perpendicular and parallel direction. The arc length is the distance between the bottom fringe of the stress cone and the point of interest. It's actually a straight line even though there is a word 'arc' in the name.  $E_{norm}$  means the absolute value of the electric field strength.

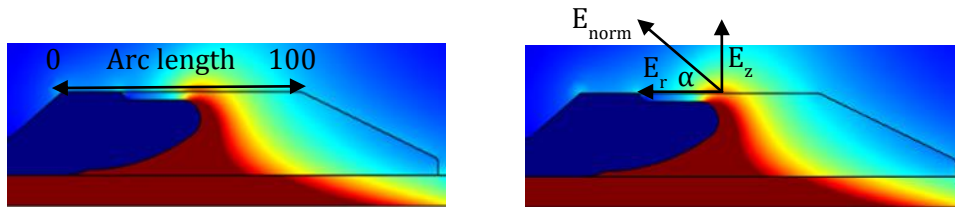


Figure 11 Illustration of the Arc length and electric field composition on perpendicular and parallel direction under 70 kV

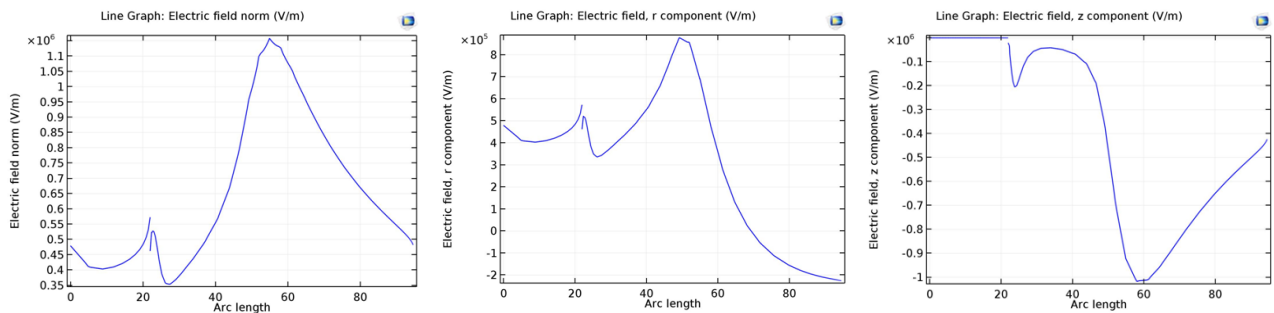


Figure 12 Electric field decompositions along the oil-rubber interface: amplitude; perpendicular; parallel

In order to know the electric field on different directions, we have to orthogonally decompose the field into two directions. One direction is in parallel with the oil rubber interface, the other one is perpendicular with the interface. As indicated in the plots,  $E_r$  is the electric field perpendicular with the interface,  $E_z$  is the electric field composition in parallel with the interface. The minus sign indicates the field pointing to the bottom of the stress cone. For the point with the highest field, the angle between  $E_{norm}$  and the oil-rubber interface can be expressed as:

$$\alpha = \arctan\left(\frac{E_r}{E_z}\right) = 36.79^\circ \quad (8)$$

This is illustrated as in the figure 12. So far, we get the information about the E-field distribution on the oil-rubber interface. Both the direction and the amplitude of the E-field are useful to build up the small scale test setup.

#### 2.4. The need of a 3D model for simulation when water droplets present

It's impossible to put a water droplet in a 2D simulation model because of the symmetric nature of 2D. This is further explained in the figure 13,

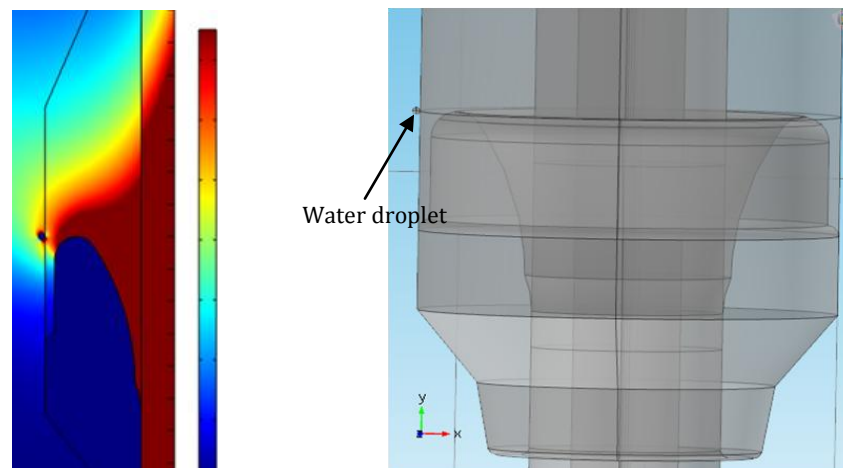


*Figure 13 Example of water droplet in a 2D model and a 3D model*

If figure on the left is the plane of a 2D model, according to axisymmetric structure, the blue dot in the figure is actually representing a tube rather than a sphere. Due to the unsymmetrical geometry caused by water content, we need to use a 3D model, as it on the right of the figure 13.

### ➤ 3D model simulation results

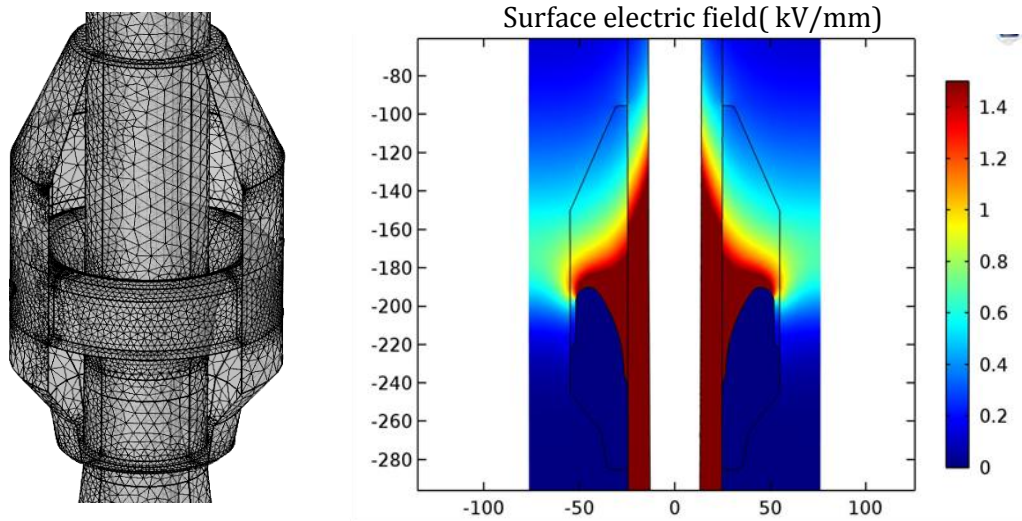


Figure 14 Electric field amplitude distribution under 70 kV from 3D model simulation(size in mm, negative sign indicates direction)

As we can see, the resulting electric field distribution from the 3D model is the same as the one from the 2D model. The maximum electric field is 1.12 kV/mm. Notice that this value is lower than the maximum value given by the 2D model, but the difference is within 2% which is acceptable.

### 2.5. Electrostatic study on the effect brought by the water droplets

A water droplet with a radius of 1 mm is put on the stress cone. Notice that the position where the droplet lands on has the highest electric field according to the previous simulation. The relative permittivity of water is 80 at 20 °C.

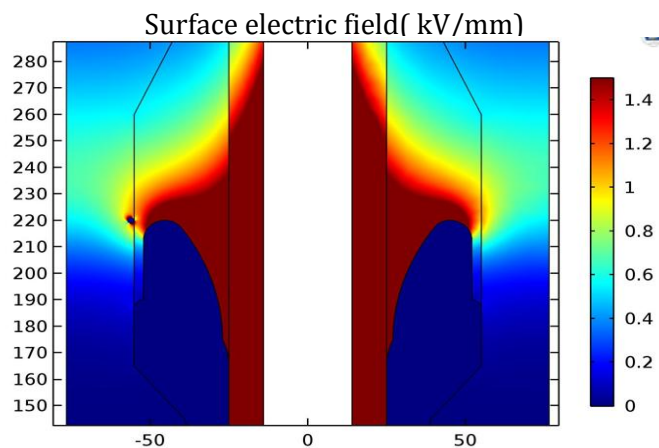


Figure 15 Electric field amplitude distribution under 70 kV with a droplet presenting on the cone surface(size in mm)

The change of the electric field after introducing the water droplet on the stress cone can be seen from the figure 15. The maximum electric field on the stress cone surface is increased to 2.68 kV/mm due to the existence of the water droplet. In other words, the maximum electric field is 2.4 times higher than before.

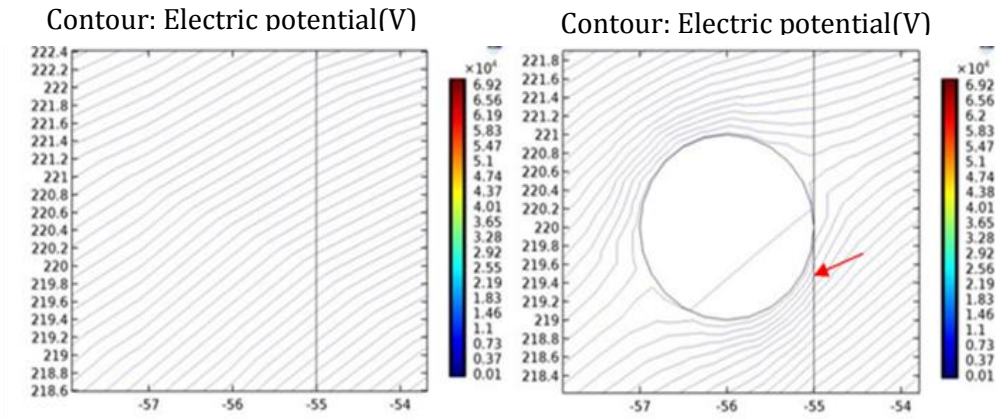


Figure 16 Equipotential line distribution, without and with water droplet under 70 kV(size in mm)

The reason for the electric field enhancement can be explained by the equipotential lines distribution, as in figure 17 and 18.

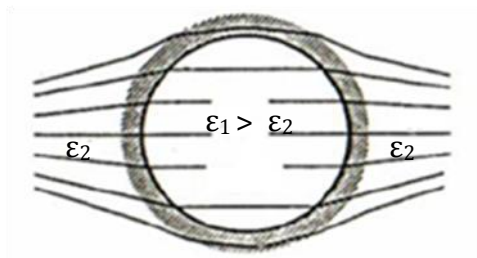


Figure 17 Equipotential lines go through different materials with different relative permittivity

The electric field distribution is decided by the relative permittivity when it comes to the interface between different material. Due to the boundary conditions, for tangential electric field

$$E_{1T} = E_{2T} \tag{9}$$

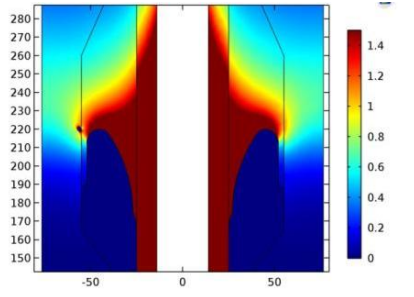
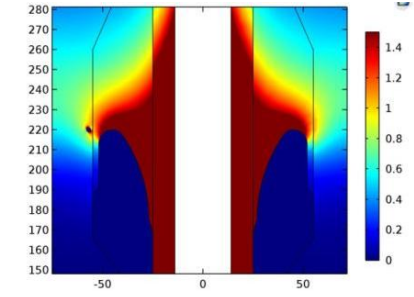
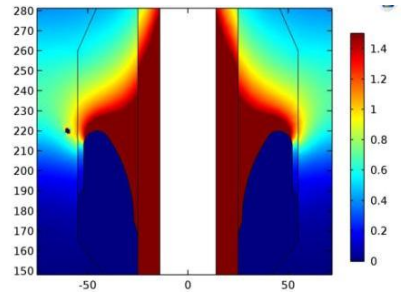
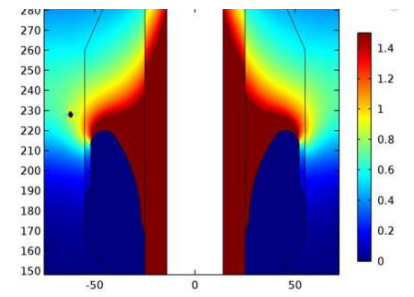
and for perpendicular electric field

$$\epsilon_1 E_{1N} = \epsilon_2 E_{2N} \tag{10}$$

The relative permittivity ratio between water and oil is 80/2,1. The large difference in relative permittivity causes field line distortion. The condensing of field lines around the brim of the droplet causes the local electric field enhancement.

➤ The effect caused by different positions of water droplet

Table 1 The effect caused by different position of water droplet under 70 kV(size in mm)

Distance from stress cone (mm)	0(perpendicular)	1(perpendicular)
Electric field distribution (kV/mm)		
Maximum E-field amplitude on stress cone surface(kV/mm)	2.68	1.15
Distance from stress cone (mm)	5(perpendicular)	10(in an angle)
Electric field distribution (kV/mm)		
Maximum E-field amplitude on stress cone surface(kV/mm)	1.10	1.10

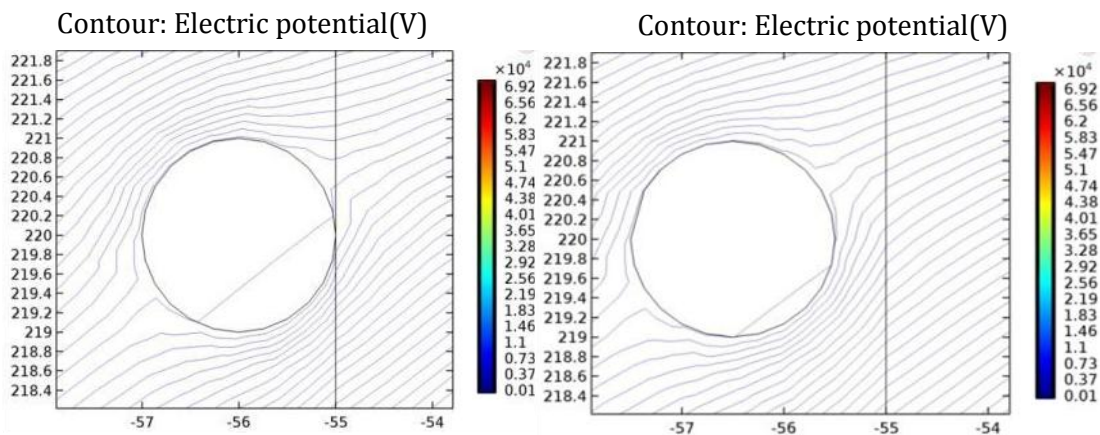


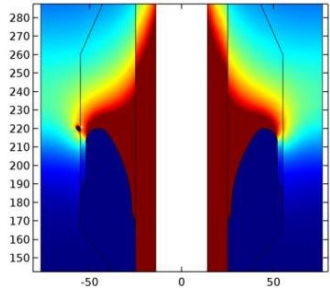
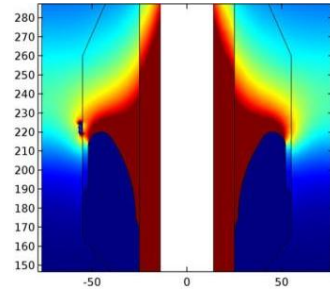
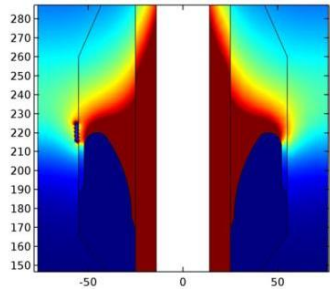
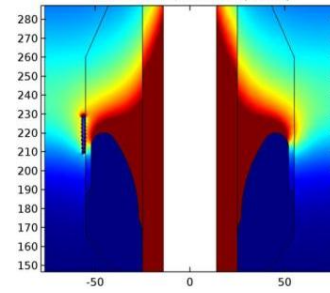
Figure 18 Equipotential line distribution under 70 kV with droplet placed at different positions(size in mm)

The maximum electric field on the stress cone decreases when the water droplet is away from the critical point. The reason for this is quite straightforward if we zoom in the electric potential lines distribution. As we mentioned before, the water droplet will cause potential lines distortion. However, if the water droplet is away from the stress cone, this field distortion will be shifted away. In other words, further the water droplet, smaller it affects the electric field on the

stress cone. It should be noted that the simulations are under static condition, so dynamic movements caused by gravity and electric force are ignored here.

➤ **The effect caused by the amount of water droplets**

*Table 2 The effect caused by the number of water droplets under 70 kV(size in mm)*

Number of droplets	1	3
Electric field distribution (kV/mm)		
Maximum E-field amplitude on stress cone surface (kV/mm)	2.68	3.36
Number of droplets	5	10
Electric field distribution (kV/mm)		
Maximum E-field amplitude on cone surface (kV/mm)	3.71	3.00

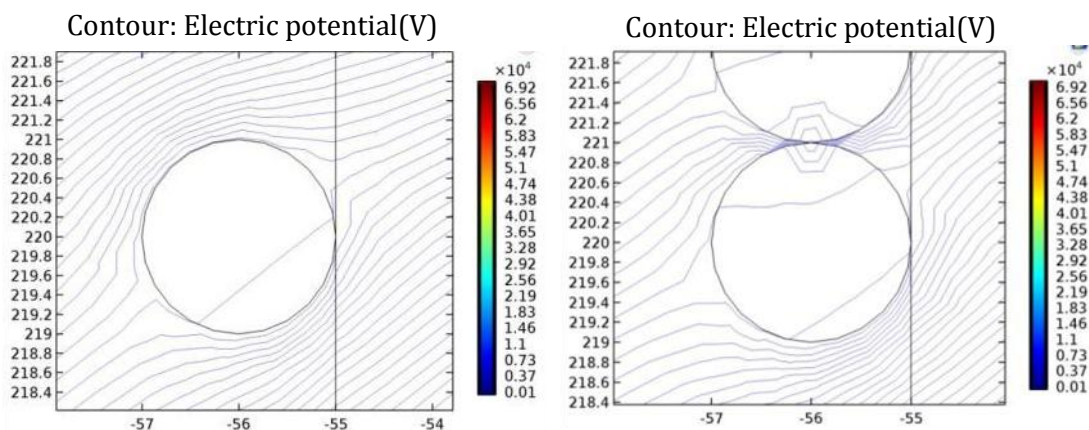


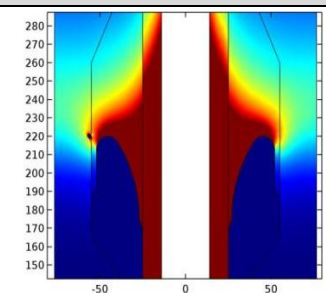
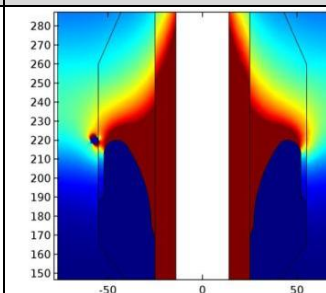
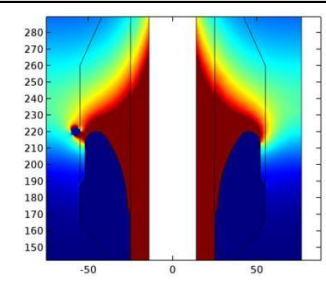
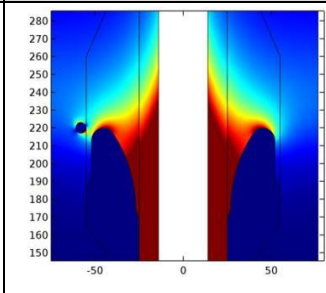
*Figure 19 Equipotential line distribution under 70 kV with different number of droplets(size in mm)*

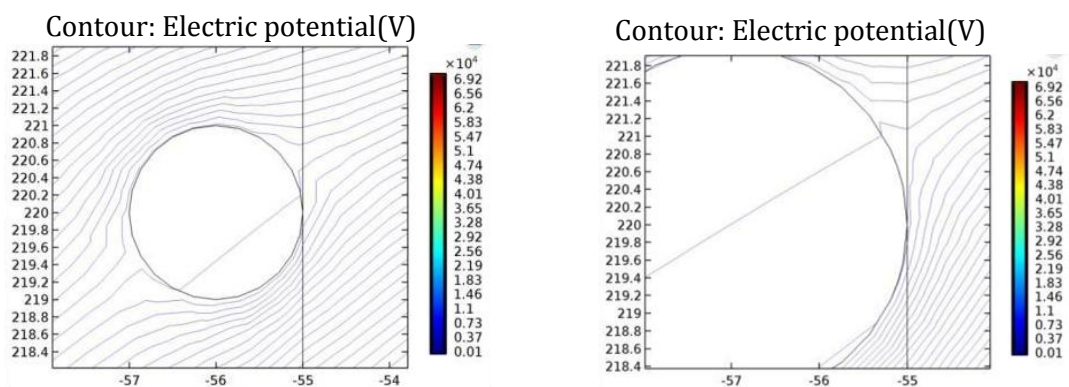
When there are more than one water droplet existing, the field lines distributes differently. As we can see from the figures, if there are another water droplet on the top of the existing one, the equipotential lines on the right part will be tilted upwards. As a result, the field lines at the corner will be condensed even more, so the electric field strength there will be increased. This doesn't mean that the maximum electric field on the stress cone will always increase with the

increase of the water droplet number. According to our simulation results, the maximum electric field strength with 7 water droplets is lower than with 3 droplets. So the maximum field strength depends on the actual field lines distribution.

➤ **The effect caused by the sizes of water droplets**

*Table 3 The effect caused by the sizes of water droplets under 70 kV(size in mm)*

Radius of droplets mm	1	2
Electric field distribution (kV/mm)		
Maximum E-field amplitude on cone surface(kV/mm)	2.68	2.72
Radius of droplets mm	2.5	3
Electric field distribution (kV/mm)		
Maximum E-field amplitude on cone surface(kV/mm)	2.30	2.30

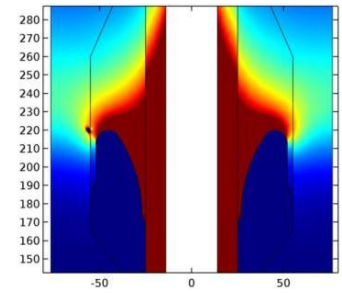
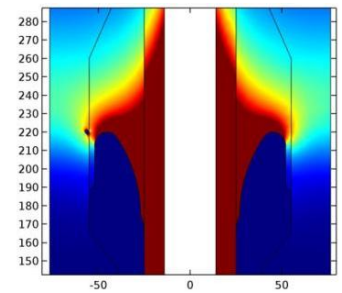
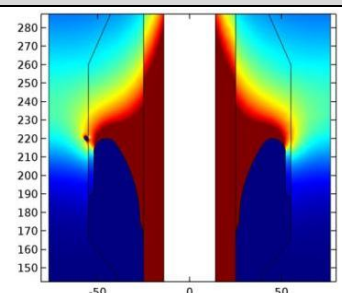
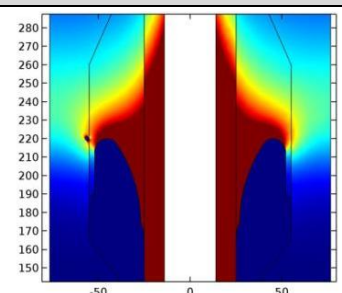


*Figure 20 Equipotential line distribution under 70 kV with different sizes of droplets(size in mm)*

Based on the figure 21, the equipotential lines are the most condensed when the radius of the droplet is around 2 mm, which gives the highest electric field. This volume of the droplet is equal to 0.1ml.

➤ **The effect caused by the relative permittivity of water droplets**

*Table 4 The effect caused by the relative permittivity of water droplets under 70 kV(size in mm)*

Relative permittivity of water droplets	80	70
Electric field distribution ( kV/mm)		
Maximum E-field amplitude on stress cone surface( kV/mm)	2.68	2.66
Relative permittivity of water droplets	60	50
Electric field distribution ( kV/mm)		
Maximum E-field amplitude on stress cone surface( kV/mm)	2.63	2.59

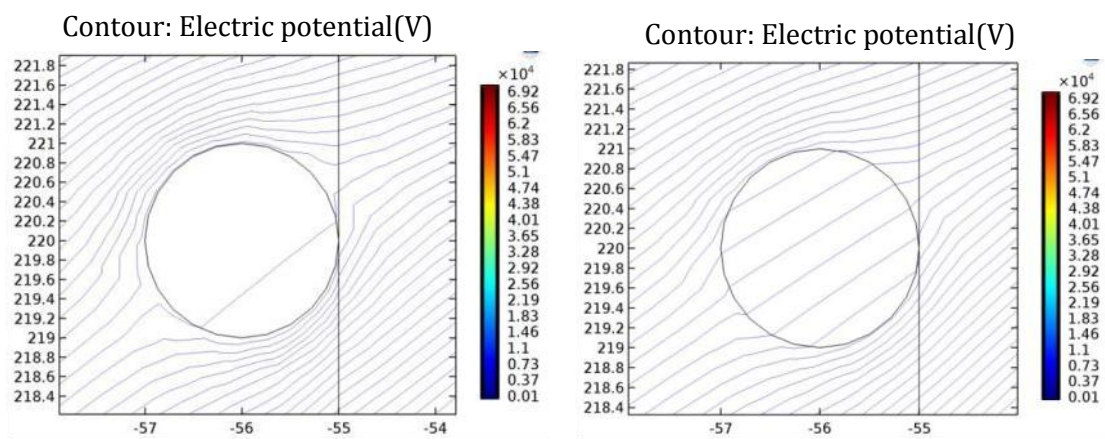


*Figure 21 Equipotential lines distribution under 70 kV with droplets having different relative permittivity(size in mm)*

The relative permittivity for oil here is 2.1, and normally this value is way below the relative permittivity of water which is around 70. As indicated in the figure 22, if the relative permittivity of the water decreases, the field lines around the brim corner will be ‘attracted’ into the water

droplet, so the potential lines will be less condensed. In the end the maximum electric field on the stress cone will be lower.

## 2.6. Electric current study on the effect brought by the water droplets

The equivalent circuits of the model are different under different study modes. It's illustrated as below.

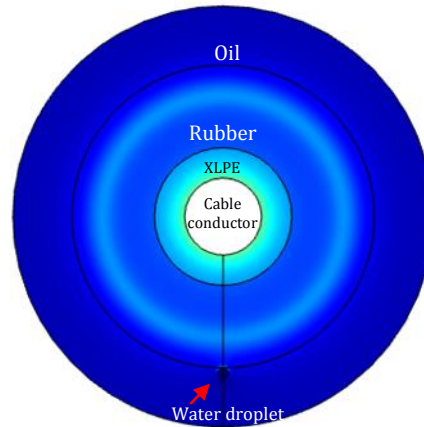


Figure 22 The horizontal cross section of the termination

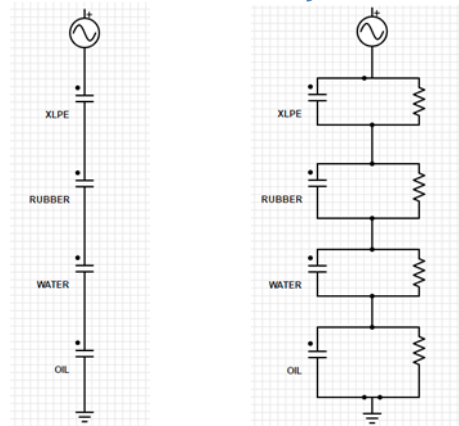


Figure 23 Equivalent electric circuits under electric static study and frequency domain study

In COMSOL, when the simulation is under electric static mode, the electric field distribution is calculated according to the capacitance ratio between different components. This is confirmed by using a simple model with different relative permittivity layers. The relative permittivity of the material is required by the simulation program to calculate the capacitance. The capacitance of a cylinder shape can be calculated by the formula. The calculation process can be found from formula 1 to 7. For the simulation under frequency domain, the conductivity also plays a role when calculating the voltage distribution. The formula for deciding the voltage distribution should be changed to the one below.

$$V_{\text{Material}} = V_{\text{Source}} \times \frac{Z_{\text{Material}}}{Z_{\text{Total}}} \quad (11)$$

In which  $Z_{\text{Total}}$  is the total impedance,  $Z_{\text{Material}}$  is the impedance of different components.

➤ **The electric field for water droplets with different conductivities under 50Hz**

*Table 5 The electric field with different water droplets conductivity under 50Hz at 70 kV(size in mm)*

Conductivity	5 S/m	0.5 S/m
Electric field distribution (kV/mm)		
Maximum E-field amplitude on stress cone surface( kV/mm)	2.86	2.86
Conductivity	0.05 S/m	0.0005 S/m
Electric field distribution (kV/mm)		
Maximum E-field amplitude on stress cone surface( kV/mm)	2.86	2.86

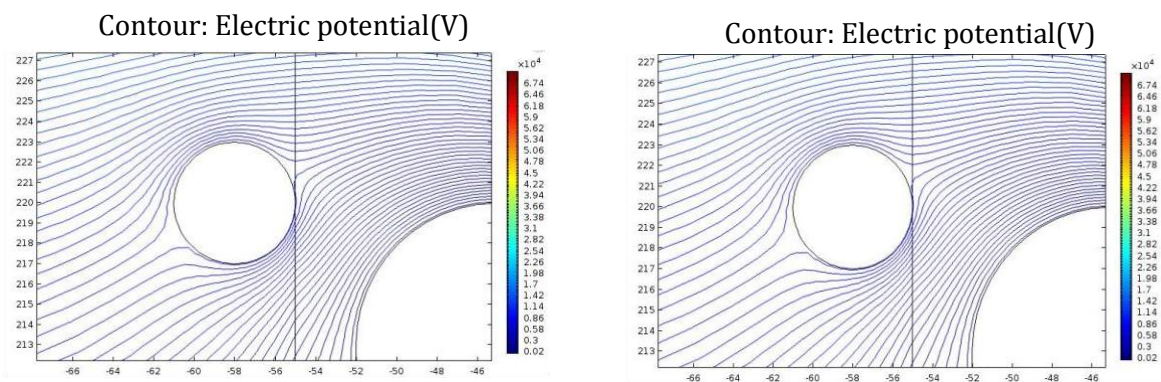


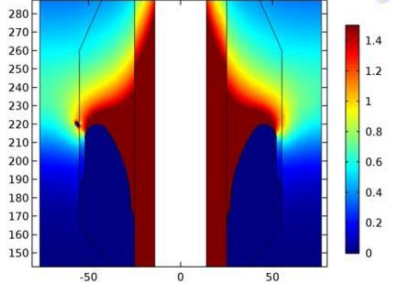
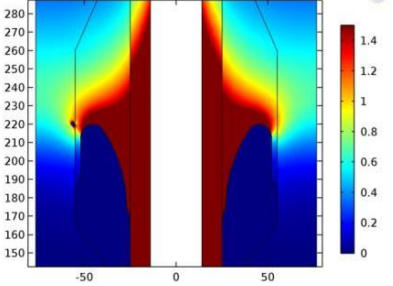
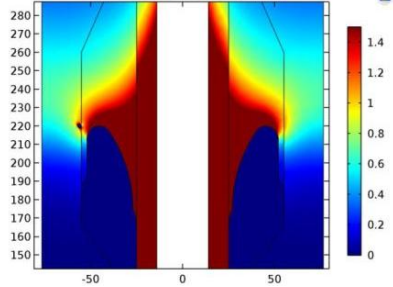
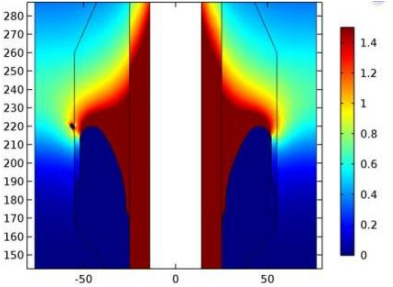
*Figure 24 Potential lines distribution under 70 kV for water droplets with different conductivities(size in mm)*

Here we compare the electric field distribution with different water droplets conductivity under 50Hz at 70 kV. The electrical conductivity of the pure water is pretty low, and it increases with the dissolution of ionic material such as salt. The sea water has a conductivity value of 5 S/m

[19], and the tap water normally has a value between  $5.00 \cdot 10^{-4}$  to  $5.00 \cdot 10^{-2}$ . Ultra-pure water has even lower conductivity, around  $5.00 \cdot 10^{-6}$  S/m. But it is normally used in semi-conductive industry. Considering the operating environment, we set the conductivity range between 5 S/m to  $5.00 \cdot 10^{-4}$  S/m. From the simulation result in figure 5, the maximum electric field doesn't have noticeable change with the change of the conductivity under this circumstance. In fact, the simulated difference is within  $1 \cdot 10^{-6}$  kV/mm, so it is negligible.

➤ **The electric field of water droplet under different frequency(0.5 S/m)**

*Table 6 The electric field of water droplet under different frequency at 70 kV(size in mm)*

Frequency	45 Hz	50 Hz
Electric field distribution (kV/mm)		
Maximum E-field amplitude on stress cone surface(kV/mm)	2.8621	2.8621
Radius of droplets mm	5 KHz	5 MHz
Electric field distribution (kV/mm)		
Maximum E-field amplitude on stress cone surface(kV/mm)	2.8620	2.8619

The increased usage of power electronic devices in the grid introduces many switching waves which results in severe stress with varied frequency on the insulating components [20]. The calculation of the component impedance also involves with frequency.

$$Z_{\text{Material}} = Z_R // Z_C \quad (12)$$

Where  $Z_R$  is the resistance  $R$ , and  $Z_C$  is the impedance of the capacitor.  $Z_C$  equals to  $\frac{1}{j2\pi fC}$ . In order to investigate the influences brought by the change of the power frequency, we did the simulation with power frequency from 45 Hz to 5 MHz. From the results above we can see the electric field difference caused by power frequency is still small but not as trivial as the conductivity simulation. The difference is around  $1 \cdot 10^{-4}$  kV/mm.

## 2.7. Theoretical highest electric field situation

Based on the simulation we have done, it is time to propose the testing condition which can represent the real situation and replicate the worse scenario.

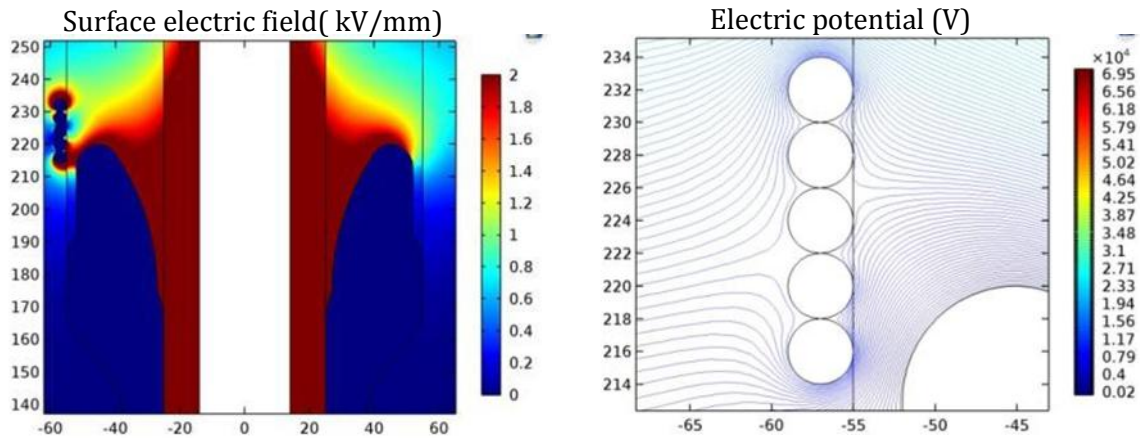


Figure 25 Scenario which produces the highest electric field strength under 70 kV(size in mm)

According to the simulation mentioned before, we may get the highest interface electric field if we put 5 water droplets around the critical points with a radius of 2 mm. The maximum electric field is 9.7 kV/mm on the stress cone. Our interests are not only on the amplitude of the electric field but also the direction of the field.

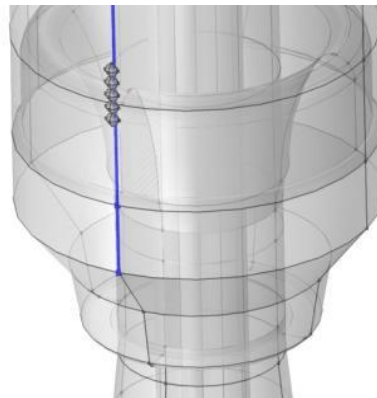


Figure 26 Electric field at one line of the stress cone under 70 kV

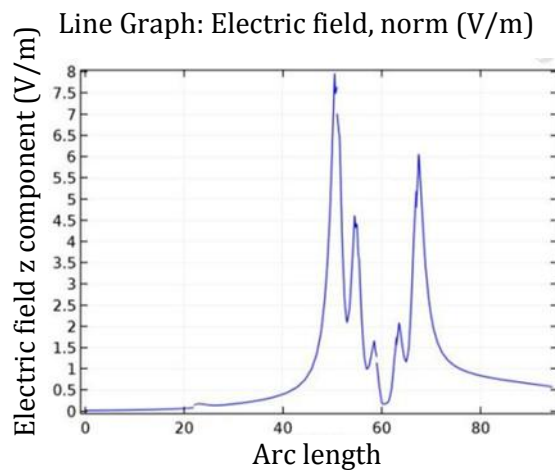


Figure 27 Electric field amplitude along the stress cone under 70 kV(size in mm)

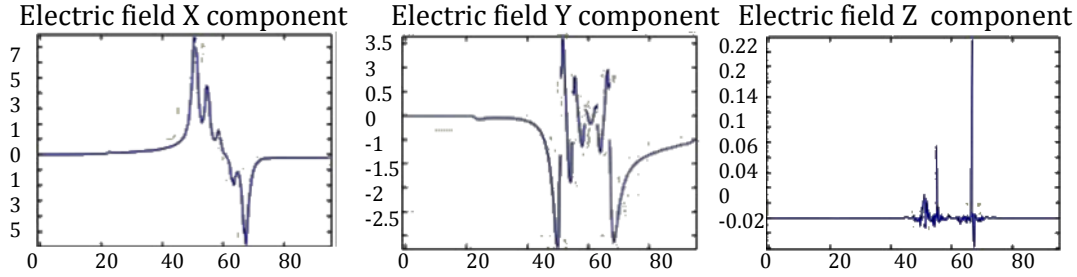


Figure 28 Electric field amplitude along the line for W Y Z direction under 70 kV(size in mm)

The electric field at all three directions can be read from the figures above. The highest field strength are  $E_x=7.64$  kV/mm,  $E_y=2.73$  kV/mm and  $E_z=0.01$  kV/mm. Although  $E_z$  is also the filed along the oil-rubber interface, but it's value can be seen as negligible compared with  $E_y$ .

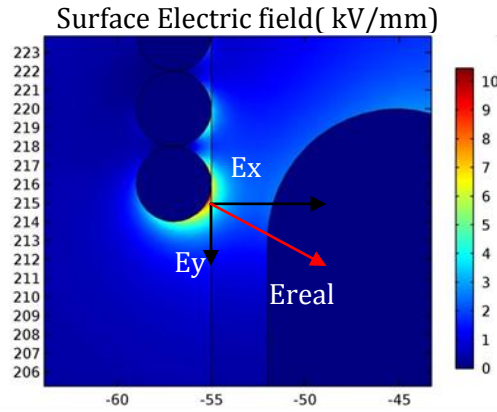


Figure 29 Highest electric field amplitude composition on perpendicular and parallel directions under 70 kV(size in mm)

Based on the simulations we did, the electric field enhanced by the water droplets along the oil-rubber interface can be as high as 2.73 kV/mm. Even though this value is below the company limit 7 kV/mm, it is already 2.7 times higher than the field without water contamination. The increase of the electric field will affect the operating life time of the stress cone [21]. The relationship between stressed electric field and insulation life time can be described as [22]

$$L = C_0 / (E - E_T)^n \quad (13)$$

In which  $L$  is the lifetime,  $C_0$  and  $n$  are the coefficients which can be derived from accelerated aging tests,  $E$  is the electrical stress on the insulation,  $E_T$  is the electrical threshold below which no degradation takes place. Based on the equation, the electrical stress has an inversely exponential manner on the life time of insulation. So trebled electric field along the oil-rubber interface will reduce the life time a lot. This increase of the filed also influence the treeing growth rate on stress cone surface [23]. The treeing growth rate is normally decided as [24],

$$t_G = \frac{k_1}{k_2(E - E_T)} \quad (14)$$

In which  $t_G$  is treeing growth time of the insulation,  $k_1$  and  $k_2$  are coefficients defined by the material. The increase of the electric field will shorten the treeing growth time.

## 2.8. Conclusion from the simulation results

Based on the simulation results, the following conclusions can be made:

### ➤ **The influential parameters**

The main parameters that affect the electric field distribution on the oil-rubber interface includes: droplets positions, the size of the droplets, the relative permittivity of the water and the number or covering area of the water droplets.

### ➤ **Field enhancement due to water contamination**

The amplitude of the electric field along the oil-rubber interface can be trebled due to the presence of water contamination. This field enhancement will decrease the lifetime of the stress cone and shorten the treeing growth time of the cone surface. In other words, the presence of water contamination on the oil-rubber interface will significantly accelerate the insulation degradation.

## 3 Small scale test setup design

### 3.1. The objectives of the small scale test

From previous analysis we know the importance of the oil-rubber interface. The need from the company is to detect the presence of water contamination on the stress cone surface. However the information we get from the simulations is not enough to well understand how things going on the oil-rubber interface, and the possibilities of detecting the presence of water contamination. The simulations can only provide a static results, so the dynamic process and physical phenomena are blinded. For engineering purpose, the simulations cannot give a hands-on experience, and its results cannot give direct indication of building up the measuring systems. Therefore we need to replicate the real situation by building up a small scale test setup. This doesn't mean the simulations are worthless. On the contrary, we need the information form simulation results to come up with the setup design.

### 3.2. Test setup design by 3D simulation

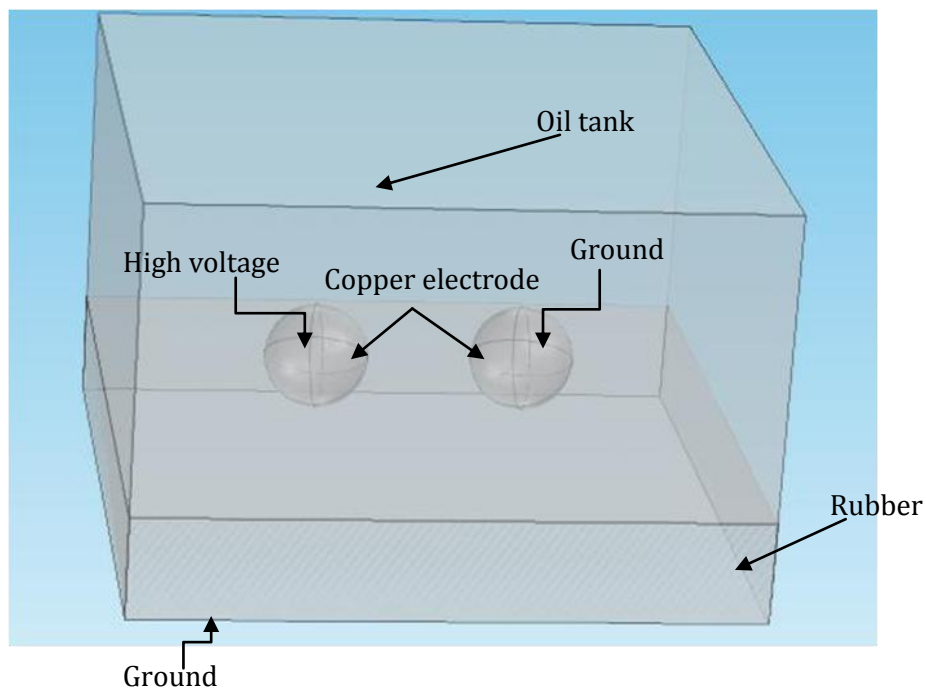


*Figure 30 Small scale test setup sample*

The most straightforward design for our test setup can be found in figure 31. The basic components in this configuration includes two electrodes, a piece of rubber. The space in between is filled with termination oil. The electrode is made by copper. The material of rubber and oil should be the same one from the a real termination. One of the electrodes is applied with high voltage, and the other one is grounded. This preliminary idea should be examined to ensure the desired electric field distribution. This can be done by using COMSOL simulation. The relative permittivity of different components is set as the same value in a real termination. The applied voltage is 1 kV.

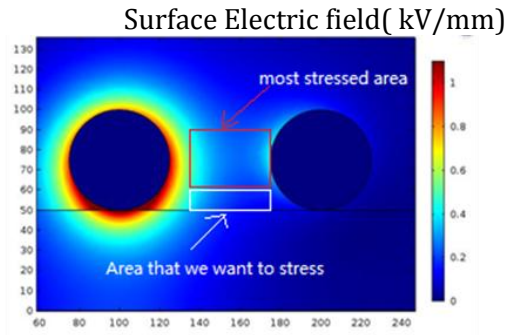


Figure 31 Simulation result of preliminary test setup under 30 kV(size in mm)

As we can see from the result above, there is a major problem that needs to be solved. In this design, the most stressed region is not rubber surface but the oil above it. Later on, this stressed region may cause unwanted PD signals. The electric field strength on the rubber surface should also be adjusted to the value we get from previous simulations. Empirically, field distribution is decided by the shape of the electrodes. Therefore we modified the shape and simulated again.

Table 7 Electric field distributions under 30 kV with different electrodes shape(size in mm)

Shape of the electrodes	Sphere	Cubic
Electric field distribution		
Shape of the electrodes	Steep slope triangular prism	Gentle slope triangular prism
Electric field distribution		

It's obvious that the trick to 'drag down' the electrical stress is to decrease the distance between the bottom parts of the electrodes and increase the distance between the tops. The triangular prism shape gives the most desirable E-field distribution, but this shape cannot be easily connected with the voltage sources and grounding lead. Instead, we came up with the boot shape electrodes.

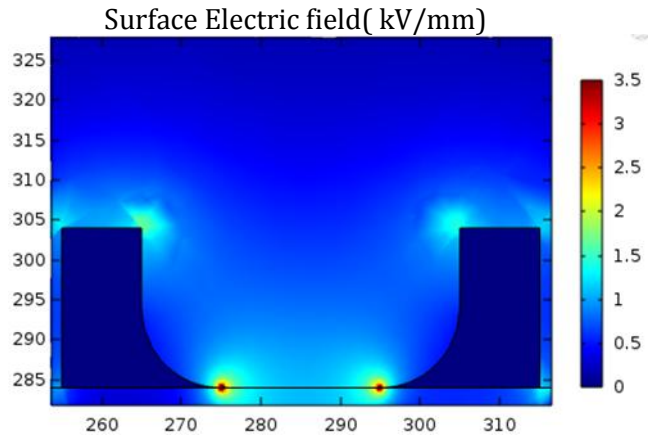


*Figure 32 Electric field distribution under 30 kV with boot shape electrodes(size in mm)*

This boot shape design can stress the rubber surface in a wanted way and is easily to connection with the voltage source and grounding lead. The sharp corners and edges would cause field concentration and create problems, so they will be avoided when it's made. Now the electrodes shape is good enough but the rubber surface still need to be revised. In a real termination, stress cone surface has a cylindrical shape instead of being flat. Even if a flat shape rubber is acceptable, it cannot be made easily. The shaving and cutting process will create a rough surface which could strongly influence the experiment results. In order to make the experiment as perfect as possible, we discussed with Prysmian and they agreed to provide a real stress cone. The relevant size of the stress cone can be found below. The designed electrodes cannot stand on the cylinder rubber surface, so we adapted the electrodes to fit with it. Finally, we can assemble our real test setup.

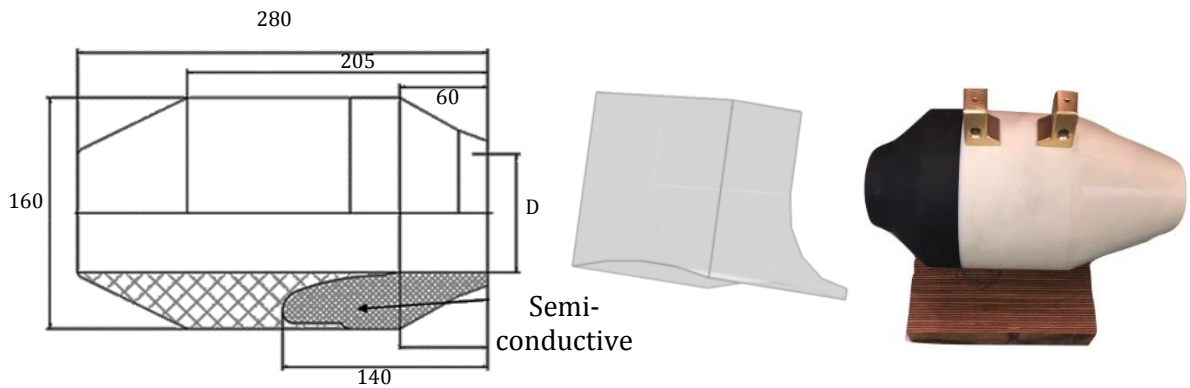


*Figure 33 Size of the cone; electrode shape; final set up`*

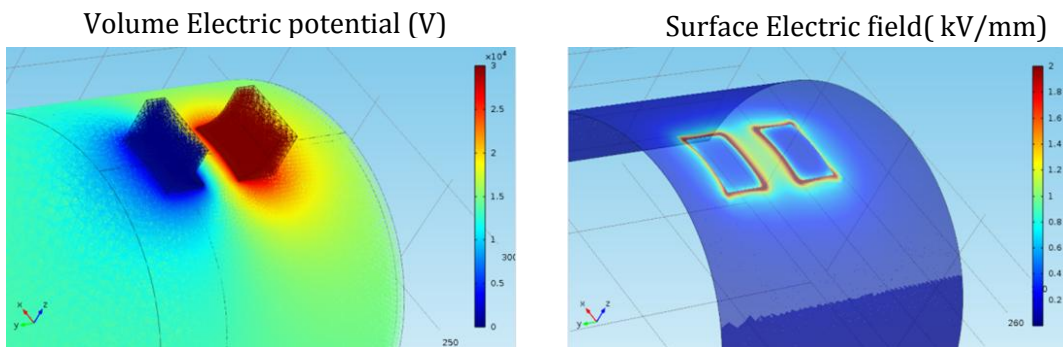


*Figure 34 The electric potential distribution and the electric field distribution of our test setup under 30 kV*

Before applying any voltage, we used COMSOL to simulate the resulting electric field. Dimensions in 3D model are the same in real test setup. Notice that the shape of the stress cone is simplified. The distance between two electrodes is 2.5cm and the applied voltage is 30 kV. Resulting E-field amplitude on the surface between the electrodes is around 1.4 kV/mm, which is within the range we got from previous simulations.

### 3.3. Real test setup construction



*Figure 35 Testing area configuration*

With all the work we have done above, it is time to build up the testing place. The testing place includes two areas, the testing area and measuring area. Between them there is an isolating fence for protection. The first priority a testing place is to make sure the safety of operators. Therefore a metal fence is needed to isolate the operator and testing area. This fence is also acting like a switch, The voltage transformer will be disconnected from the power source if the fence is open, in case there is people in the testing area. This mechanism greatly reduces the chance of unintentional energizing. The fence also prevents other people getting into the ongoing experiments.

### ➤ Testing area description

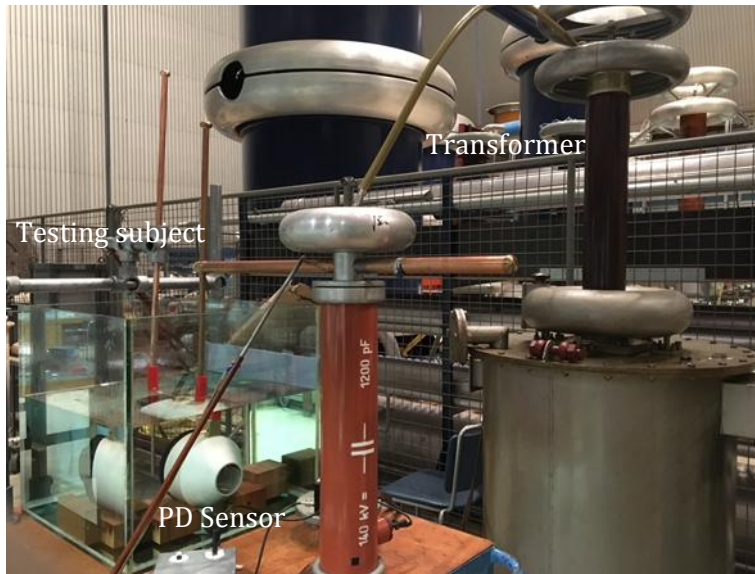


*Figure 36 The components in the testing area*

The testing area contains of a high voltage transformer, the main testing subject and a partial discharge sensor. The transformer has a ratio of 1/500 and is corona free up to 60 kV, which is quite well above 30 kV. In order to prevent high frequency noise getting into the PD sensor, we put a HF noise filter in between the transformer and the voltage divider. The connection cable is concentric high voltage cable with aluminum core. The measuring capacitor is 1200pF. In order to replicate the real situation, the main testing components are immersed in the oil aquarium, as in the figure below. The stress cone is supported by the wood below. This supporting wood is from a voltage transformer which could give both stable fixation and electrically isolate the cone from the bottom of the aquarium.

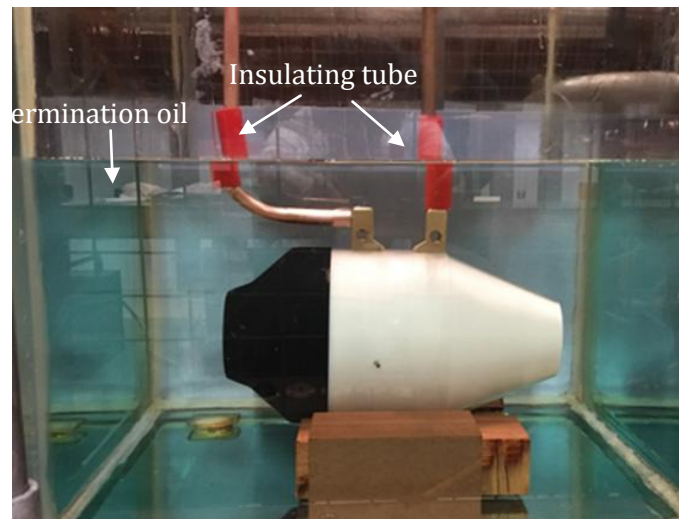


*Figure 37 The main testing subject in the oil aquarium*

The aquarium is poured with the termination oil. This is the same oil being used in the real termination. The breakdown strength of the oil is 12 kV/mm. The plastic tubes coaxing around the bottom conducting bar prevent the partial discharge along the oil-air interface, in other words the surface of the oil.

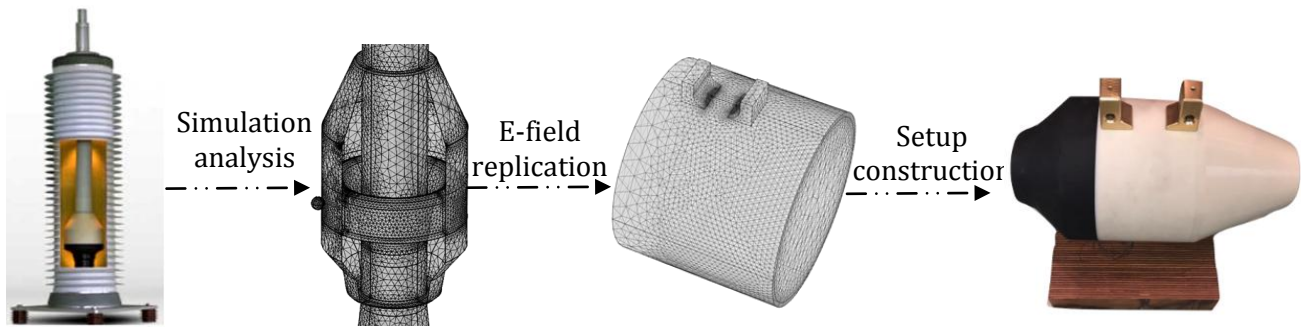


*Figure 38 The logic of test setup designing*

The logic flow for designing the test setup can be found in the figure 38. That's how we build it up step by step.

➤ **Measuring area**

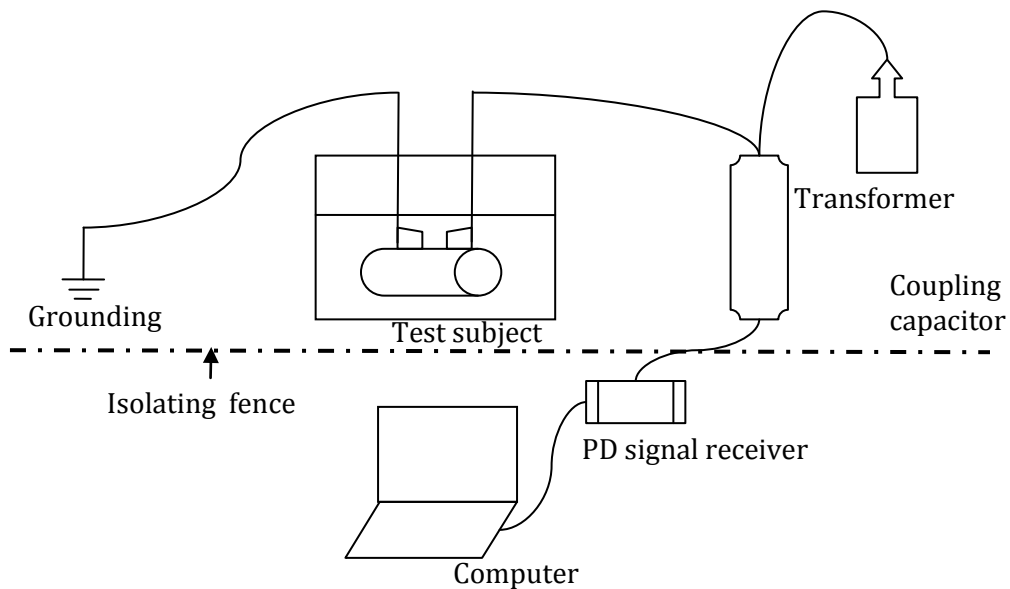


*Figure 39 Scheme of testing area and measuring area*

On the other side of the fence, there is a monitoring screen. The screen is connected with a digital video camera which provides real-time image in the testing area.



*Figure 40 The measuring area*

The measuring area is for operators to manipulate the voltage applied on the testing subjects and monitor the PD activities. The voltage regulator is used to set the voltage level. By rotating the handheld clockwise, the voltage can be increased and vice versa. There is a current relay inside the voltage current monitor, which aims to trip the switch when there is breakdown in the test. This protection device is put in between the power source and the voltage regulator. The PD receiver captures the signal from the testing subject. The connection of PD receiver can be seen in figure 42.

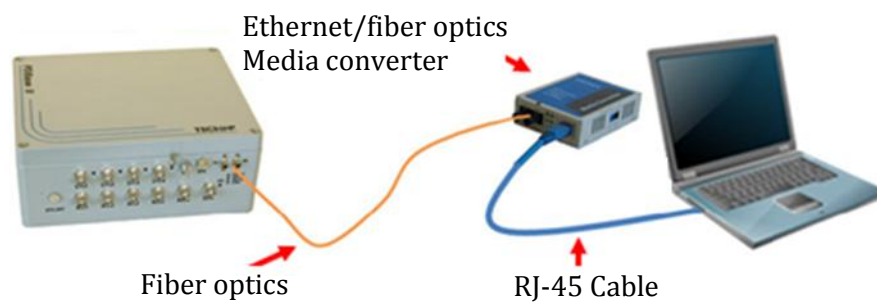


*Figure 41 connection between the PD receiver and the computer*

The operator can use the software installed on the computer to monitor the PD activity and analyze the wave form and PD pattern. This part will be elaborated in the next chapter.

# 4 Partial discharge measurement

## 4.1. PD detector explanations and detecting circuit

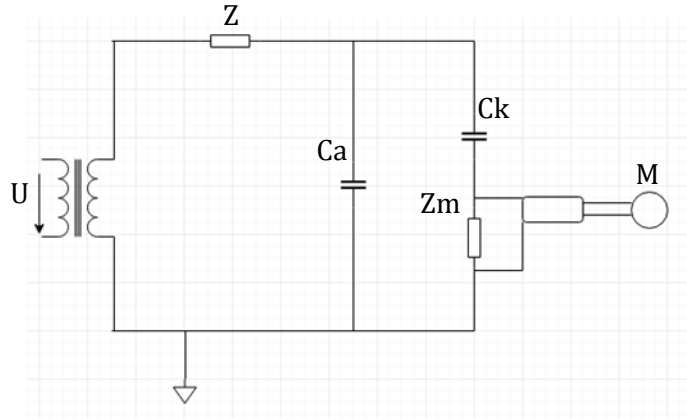


Figure 42 Partial discharge detection circuit illustration

Insulation degradations are usually evaluated by either partial discharge measurement or dielectric losses measurement [25]. Partial discharge is regional breakdown on the insulation which is regarded as an indication of insulation degradation. There are three types of partial discharges: internal discharge, surface discharge and corona discharge. Internal discharge happens inside the insulation material. Surface discharge is the discharge along the insulation surface. Corona discharge is the breakdown in the air due to protrusions or rough surface of the electrodes. Our goal is to link PD activities with the presence of water contamination. So in the end, the company can use this as references to detect water contamination in terminations by measuring PD.

The basic partial discharge detecting circuit can be found above. In which the voltage is provided by the power source and leveled up by the transformer.  $Z$  represents the impedance of the testing circuit.  $C_a$  is the testing subject.  $C_k$  is the coupling capacitor which completes the circuit for passing through the discharges.  $Z_m$  is the measuring impedance and can provide voltage pulses to the  $M$ , which represents measuring and monitoring system [3]. The real elements mentioned in the illustration can be found in the previous chapter. In our experiment, we use Techimp PDBasell® for the measuring part. This device cannot only provide online PD monitoring but also acquire the wave form and analyze the PD pattern afterwards.

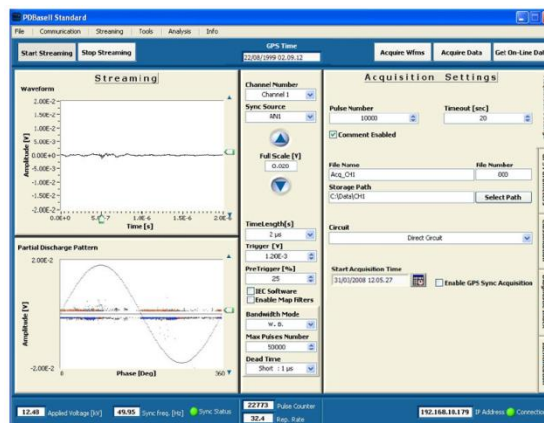
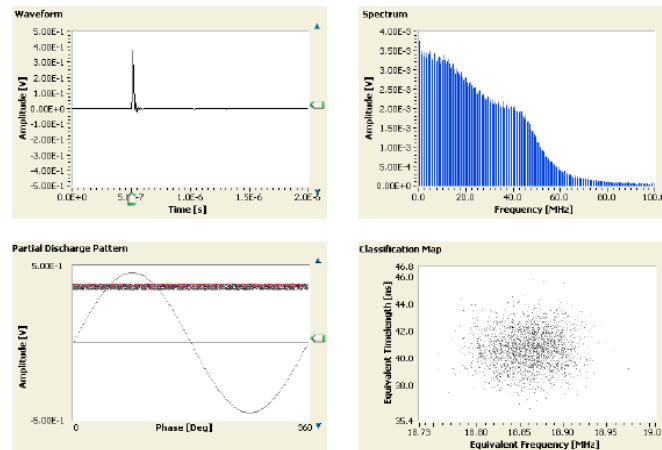


Figure 43 Main operation window of the PD detector

In order to get the best wave shape of the PD, the operator can manipulate the trigger level, bandwidth and time length. Pulses can be depicted with four different visualizing forms: pulse waveform, pulse spectrum, PRPD pattern and classification map. Waveform graph displays the pulse waveform in the time domain. Spectrum graph provides the pulse power spectrum in the frequency domain. PRPD Pattern graph shows a large amount of acquired pulses relating their amplitude with their phase. Classification Map shows the acquired pulses classified by equivalent time length and the equivalent frequency. The formation in the classification map indicates certain type of PD, so it is regarded as the fingerprint of PD pattern.



*Figure 44 Different visualizations of the PD*

All of the visualization methods can be used to identify the PD patterns. The decision making process can be done by either internal software or by operators themselves.

## 4.2. PD sources in the test setup

Our intention is to investigate the phenomena on the oil-rubber interface. In order to make sure the observed partial discharge activity is actually from the interface, we need to assure the other parts of the setup is PD free up to certain voltage level. In our test setup, there are four potential sources that may give PD signals and influence the test results.

The first possibility is from the high voltage transformer [26] [27]. The transformer we use is noted as PD free up to 62 kV. And we did the PD test with the transformer only, which showed that it is PD free up to 60 kV. This suggests that we would get partial discharge from the transformer if the output voltage is above 60 kV. Later on, when we decide the other PD sources, the applied voltage should always be lower than 60 kV.

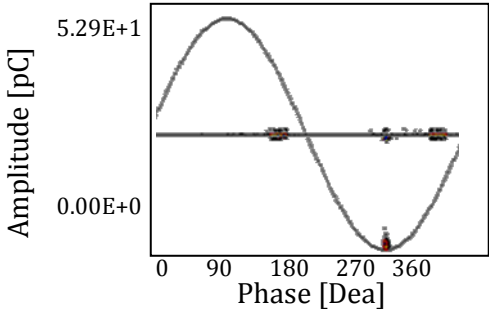
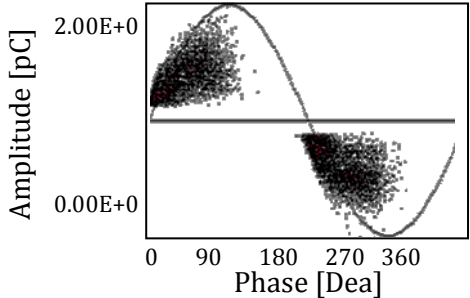
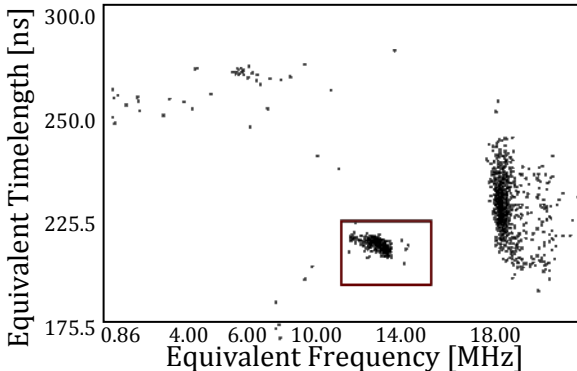
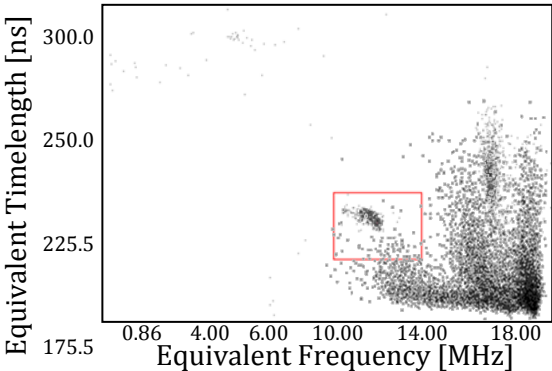
From the top to the bottom, the second potential PD source is from the conducting bars on both high voltage side and grounding side. The PD inception voltage on the bars can easily be decreased by putting the toroid cap on the top of the bar. This cap smoothens the E-field on the top of the bar and therefore increase the corona inception voltage [28].



Figure 45 Toroid cap on the top of the conducting bar

However, after putting on the toroid cap, the conducting bars are still not PD free due to the imperfect manufacturing along the surface. The figure below shows the corona on the conducting bar at 52 kV. The location of the corona is tracked by the noticeable sound it generates [29]. As we can see from the PRPD pattern we got, it has typical corona discharge shape, which means the discharge only appear on the one half of the sinusoidal wave. Due to the corona from the conducting bar, now the testing voltage is further limited to 52 kV.

Table 8 PD sources in the test setup

PD source	Corona on the conducting bar	Oil-air interface
Measurement		
PD pattern		
Classification map		

Besides the transformer and conducting bars, the oil-air interface is also vulnerable when it comes to partial discharge [30]. As we can see from the measurement done below, when the applied voltage was increased to 35 kV, there was distinctive discharge pattern in the test setup. In order to locate this PD source, we put on two insulating tubes to cut off the discharge path. We repeated the measurement under the same condition. The result is presented below.

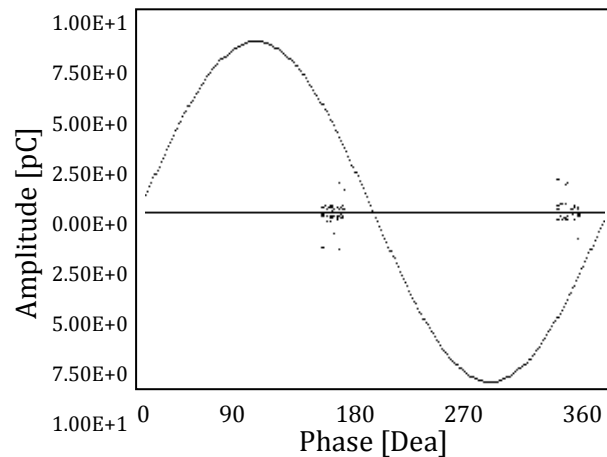


*Figure 46 The partial discharge gone after putting insulating tubes*

As it's depicted on the figure 47, the PD activities are greatly reduced by the insulating tubes. Until now, the test setup is PD free until 52 kV. Another possible PD source is the termination oil. This oil has a formidable insulating property. Under the testing voltage, it is unlikely to have any PD in the oil. In order to confirm that the oil is PD free in our setup, we did the experiments under several different conditions. First we set the distance between the electrodes to 3cm. Given the dielectric breakdown strength of the oil is 12 kV/mm, this distance can bear a voltage around 360 kV with homogeneous electric field. The test was done as follow: the applied voltage started from 0 kV and gradually increased to 50 kV in a fix step of 5 kV for each 5 minutes. No discharge activity can be found under this circumstance.

After the test mentioned above, the distance between the electrodes was decreased to 1 cm. A breakdown happened in the oil between the electrodes when the voltage reached 39 kV. The intensified electric field around sharp edges and corners contributed to the breakdown. The breakdown in the oil creates burnt pollution which may defect our measurements [31]. In order to smoothen the electric field near the corner and sharp edges, the copper electrodes were modified after the test in the oil.

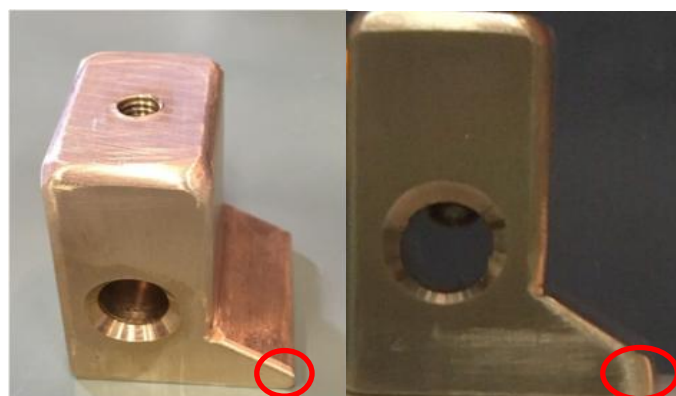


*Figure 47 The electrode before and after the modification*

The radius of the corners were enlarged from 1mm to 3mm, and all the edges were polished further.

Now we are sure that the whole test setup is PD free until 52 kV. If we put the electrodes on the rubber cone, the only possible PD source would be from the oil-rubber interface.

### 4.3. PD on the oil-rubber interface

The dielectric strength of the interface is much more lower than the strength from any of the composing materials [32]. In our case, the dielectric strength of the oil-rubber interface is roughly 20% of the termination oil. Given the short distance of the electrodes and the relatively protruding toe shape, there might be chances to have PD or breakdown on the oil-water interface even without any water content. Therefore it's necessary to guarantee that the oil-rubber interface is PD free before introducing any water content.

The tests were done as follow: the distance between the electrodes was set to 2.5cm and 1cm. For each distance, the applied voltage started from 0 kV and increased in a step of 2.5 kV/2mins to 50 kV. The reason we decreased the voltage step is to get more precise result and prevent unintentional breakdown. The PD activities were monitored and the results were recorded and presented in the table below.

*Table 9 PD inception voltage on the oil-rubber interface without water content*

Electrodes distance	2.5cm	1cm
PD inception voltage	No PD up to 50 kV	No PD up to 50 kV

As it's mentioned in the table, there was no PD activity on the oil-rubber interface if no water content involved. This confirms the great insulating properties of the oil and the usefulness of electrodes re-shaping. It should be noted that the oil-rubber interface is PD free only under certain circumstances. If there is a large amount of air bubbles near the testing region, internal PD activities may appear. The air bubbles could be introduced during the hands-in adjustment of the electrodes in the oil. Even though it's unpreventable to introduce air into the oil, we should always keep the influence from air as low as possible [33].



*Figure 48 Syringe used for injecting water droplet*

### 4.4. PD on the oil-rubber interface with water droplets

After performed all the tests mentioned before, the test setup is PD free up to 52 kV. Now it's time to put in water content into the testing region. The experiments with water contamination are divided into two groups, the water droplets experiments and the water emulsion experiments. The water droplets tests are performed according to the size and the number of the droplets. The water used in the tests is tap water. The relative permittivity under 20 °C is 80 [34] and the conductivity is around 45 S/m [35].

#### ➤ Experiments with big size water droplets

We first started with the large size of water droplet. The droplet is injected by a 5ml syringe. By using this relatively big syringe, a water droplet with a size of 0.2ml can be produced. As in the figure 10, the droplet was injected into the region and landed on the stress cone surface.

Table 10 The change of the droplet formation with time

Formation of the droplet	Landing	Deformation
		
Formation of the droplet	Disintegration	Touching
		
Formation of the droplet	Bridging	Breakdown
		

Due to the gravity and cylinder shape of the stress cone, the droplet was slightly elliptical at the beginning. The applied voltage was slowly increased from 0 kV, in a step of 2.5 kV/2minutes. The shape of the water droplet was continuously changing under the electrical stress. When the voltage reached 15 kV, the water droplet was elongated towards HV electrode. The tip on the right fringe of the droplet was about to disintegrate. The critical field strength to cause the deformation of water droplets is given below [36].

$$E_{\text{critical}} = 0.64 \times \sqrt{\frac{\gamma}{2\varepsilon_2\alpha}} \quad (15)$$

In which,  $\gamma$  is the surface tension of the droplet,  $\varepsilon_2$  is the relative permittivity of the oil and  $\alpha$  is the radius of the droplet [37]. Under this critical field strength, the tips of the droplet will be unstable. This is a rough formula which indicates the factors influencing the deforming process. As we can see, the larger the droplet the easier it is going to deform. A more detailed description of this behavior can be found in the paper [38]. From the figure above we can see the water droplet was deformed a lot and the tip were attracting to the HV electrode. The tip of the droplet was almost touching the electrode. After touching the HV electrode, the droplet was charged and maintained the same electric potential with the HV electrode. The electrical force now attracts the droplet to the grounding electrode [38]. It should be noted that there was a fine water string

which connected the droplet with the HV electrode. In other words, the droplet is still at the same electrical potential with the HV electrode.

The whole droplet was totally stretched like a tube when it was moving to the grounding electrode. The HV and grounding electrodes were about to be linked by the water droplet. Or we can say, a breakdown was about to happen. Finally, as we expected, the elongated water droplet bridges the HV electrode with the grounding electrode and resulted into a breakdown. The strong discharge of the breakdown released big amount of power and caused regional burning of the oil. The mixture of the burning gas and water evaporation went up to the surface of the oil. As in the figure below. The whole process of this experiment can be divided into 4 parts: attracting to the HV electrode, electrifying, moving back to the grounding electrode, and bridging. The whole process was not only monitored by the camera but also by the PD receiver. During our measurements, there was no PD signal before the electrodes were bridged. Only at the moment before the breakdown happened, there was a noticeable PD signal. Even though the breakdown was in a very short time, the process is still complex [39].

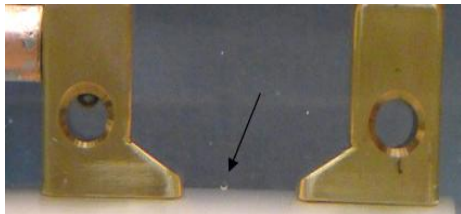
➤ **Experiments with small size water droplets**

By using the big size droplet, the experiment amplifies the movement of the smaller water droplets and indicates how it looks when the water droplets are under electric field. But in real termination operations, it is unlikely to have droplets as big as that. So we would like to do the experiments with smaller droplets. This time we used a smaller size syringe, a 1ml one. By using this one, the droplets with a size of 0.05ml can be made. Before putting the droplet into the target region, we first rotated the stress cone and cleaned up the breakdown oil- water mixture by a syringe. The new droplet now can be put on an unstressed area with clean ambient oil.

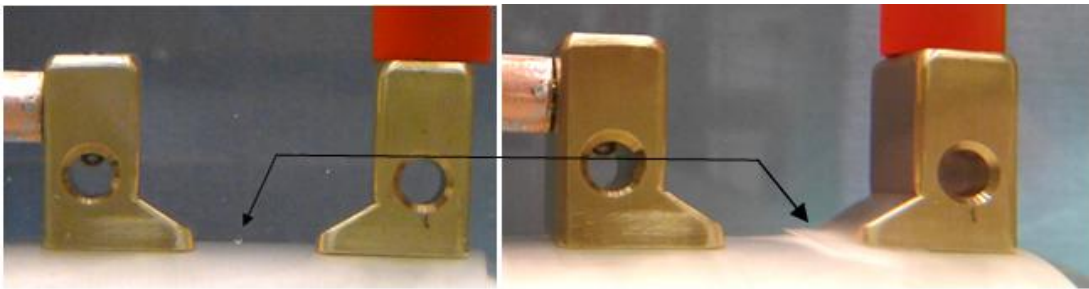


Figure 49 1ml syringe

Table 11 The change of the smaller droplet formation with time

Formation of the droplet	Landing	Disintegration
		
Formation of the droplet	Disintegration	Cotton look
		

The applied voltage started from 0 kV and was increased in a step of 2.5 kV/2minutes. The shape of the droplet got flatter when the voltage reaches 20 kV. At 22.5 kV, there was noticeable movement of the water droplet. The right tip of the flat droplet is disintegrating at this voltage level. With the increasing of the applied voltage, the disintegration continued. It looks like the tip of the water droplet is extracted out like the silk. During this extracting process, the water droplet was gradually disintegrated. When the very front part of the droplet was touching the HV electrode, the tip on the other end was stretching towards the grounding electrode. The droplet was pulled by two forces in the opposite directions. Due to the smaller size, however, it was impossible for this droplet to bridge the electrodes. In the end, the whole droplet will be like silk. The changing forms of the droplet is the result from the applied electrical stress. The water particles became smaller and smaller and they were moving to the HV electrode. Eventually all the water particles gathered around the HV electrode, and the water became like a cloud of cotton.



*Figure 50 The water droplet eventually becomes like a thin layer of cotton*

Besides observing amazing shape change of the water droplet, the PD activity was also monitored in the same time. There was no PD activity during the disintegration of the droplet. When the voltage was increased to 45 kV, the HV electrode was surrounded by the silk form of water and there was PD signal with amplitude of 9pC. The figure below shows the PD pattern and classification map of this PD signal. After 2.5minutes, the PD signal was gone when the voltage reached 47.5 kV. The test was repeated the other day. The PD inception voltage for the repeated test is 44 kV with an amplitude of 7pC. And the signal only lasted for 2minutes.

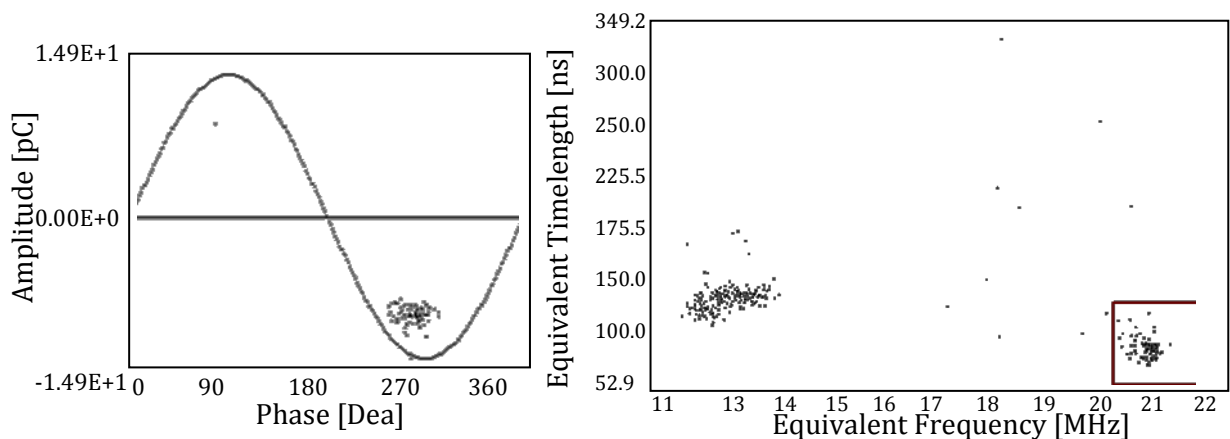


*Figure 51 PD signal for single water droplet at 45 kV*

Notice that the most part of this PD signal is on the negative half of the sinusoidal wave, which is similar with the corona. But they are totally different if we look at the frequency domain. The corona on the conducting bar has a frequency of 12MHz while the PD here has a frequency of 21MHz. This partial discharge pattern can be regarded as internal discharge in the oil due to water contamination. But a complete description for this PD activity requires more data [40].

From this case we can see that why the classification map is regarded as the fingerprint of the PD.

From the experiments above, we know the general movement and deformation of water droplets under electrical stress. The change of the droplet cannot be detected by PD receiver. Only when a stable cotton form of water was formed can we capture some PD activities. But the PD signal didn't keep for a long time.

#### 4.5. Tests on the oil-rubber interface with oil-water emulsion

##### ➤ Preparation of water-oil emulsion samples

From the previous work [7], we know that, besides the droplet, oil-water emulsion also, and more often, exists in the operating termination. This emulsion form of water contamination is an evenly distributed mixture of water and oil [41]. There are several ways to get this water-oil emulsion. For example, the emulsification can be done by ultrasonic sound bath [42]. Ultrasound-made emulsions are less poly-dispersed and more stable, but the process takes time. The emulsion can also be made by using climate chamber. After setting up the ambient moisture level, one can put the unsealed clean oil sample in the chamber. After long time, the wanted emulsion can be made [7]. Another common way of making emulsions is using emulsifier [43]. This additive is widely adopted by chemical industry, especially in fuel industry [44].

The methods mentioned above are not easy to implement. For qualitative investigation, a rather simple way of emulsifying can be chose. It is based on the fact given by the former researcher [7]. The procedure is described as follow: inject water droplets into the oil, heat up the oil to around 90°C and wait for more than 8 hours, then cool it down to the room temperature. After it gets to the room temperature, an evenly mixed water-oil emulsion sample can be created. The water content level in the emulsion is obviously determined by the amount of droplets that are injected. The heating time is decided by the initial droplet size. The smaller the droplet size, the shorter it needs to be heated. The water used here is tap water. Under different operating environments and installation conditions, the water content levels in the termination can be different. In order to know the differences brought by water levels, we prepared five water-oil emulsion samples. The containers we used are plastic cans. The smaller size of cans is 90ml, and the big one is 220ml.



*Figure 52 Prepared water-oil emulsion samples before getting heat up*

The relative water contamination level is decided as follow. The formula for calculating the water concentration P in ppm, parts per million, can be written as [45].

$$P = \frac{\text{Mass}_{\text{water}}}{\text{Mass}_{\text{oil}}} \quad (16)$$

The density of the oil is 0.893 g/cm<sup>3</sup>. So for 90ml oil, the mass is 80.4g. The smallest amount of water can be ejected by syringe is 0.01 cm<sup>3</sup>. So the water concentration is

$$P_1 = \frac{\text{Mass}_{\text{water}}}{\text{Mass}_{\text{oil}}} = \frac{0.01\text{g}}{80.4\text{g}} = 124\text{ppm} \quad (17)$$

Consider the moisture leakage during the heating process also for easy calculation, the water concentration in this sample can be taken as 100ppm. The acceptable moisture level in the termination industry is around 30 ppm. 100 ppm is quite higher than this limit. Since the minimum amount of water is set, we have to use a larger container in order to get a moisture level lower than 100 ppm. For the larger container we used, if the injected water is 0.01ml, the resulting water concentration is 50 ppm. In our test samples, the water concentration of five cans are 50ppm, 100ppm, 300ppm, 500ppm, and 700ppm.



*Figure 53 The oven for heating up the water-oil emulsion cans*

From the glass window of the oven, we observed the development of the emulsification. At the beginning the droplets sank to the bottom since they have a higher density than oil. When they were in the oven and heated up to 80 degrees, the droplets started to disintegrate into even smaller droplets. The oil has a lower viscosity when at the higher temperature [46]. The smaller size of the droplets were moving around due to the thermal fluid at 90°C. After 12 hours, the water droplets were mixed with the surrounding oil. After cooling down, this mixture became to a stable colloid. The stability of this mixture depends on the moisture level [47].



*Figure 54 The examples of resulted water-oil emulsion*

#### ➤ **PD measurement with water-oil emulsion**

We started with the 50ppm sample. The emulsion was injected into the stress cone surface by a syringe. In order to get rid of the air bubbles introduced by injection, we have to wait for 2 hours before the measurements.

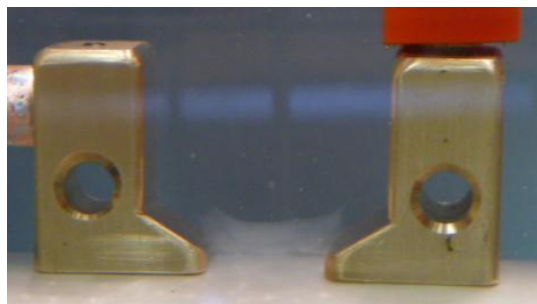


*Figure 55 The water-oil emulsion layer on the stress cone surface*

The injected emulsion formed a layer on the stress cone surface. The applied voltage started from 0 kV, and was increased in a step of 2.5 kV/2minutes. The results of the experiments are presented in the table below.

*Table 12 The water-oil emulsion experiments*

Water level PD activity	50ppm	100ppm	300ppm	500ppm	700ppm
PD inception voltage	45 kV	45 kV	42.5 kV	40 kV	40 kV
PD extinction voltage	30 kV	30 kV	32.5 kV	32.5 kV	32.5 kV
PD amplitude	6pC	7pC	6pC	7pC	6pC
Frequency of occurrence per hour	≤1	2	3	5	5

From the results, the PD inception voltage is slightly decreasing with the increase of the moisture level in the oil. Higher moisture level provides more water molecules which can cause PD, so the inception voltage is lower. But the difference in the inception voltage is not as large as we expected considering the big variance in the moisture levels. The differences in the PD extinction voltages and the amplitude of the PD are also very small.

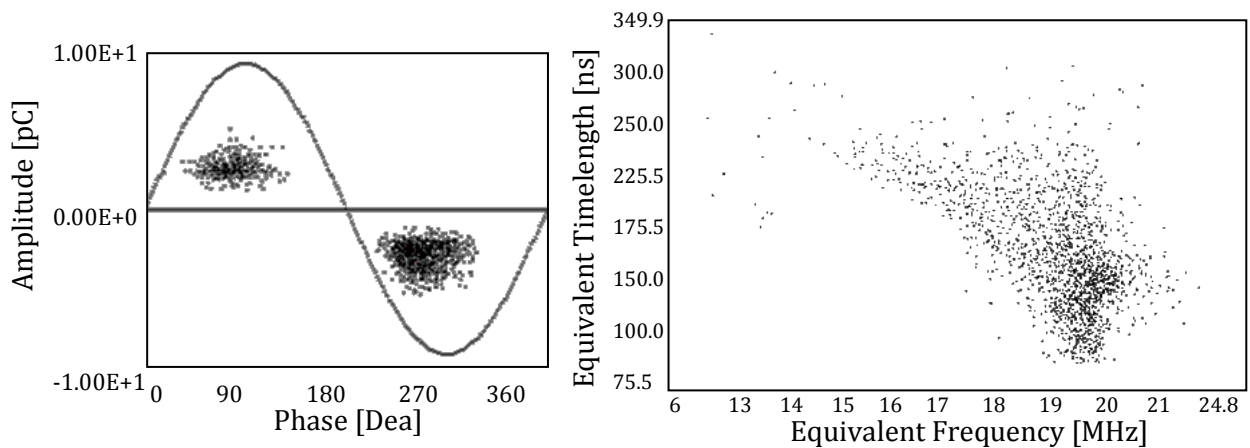


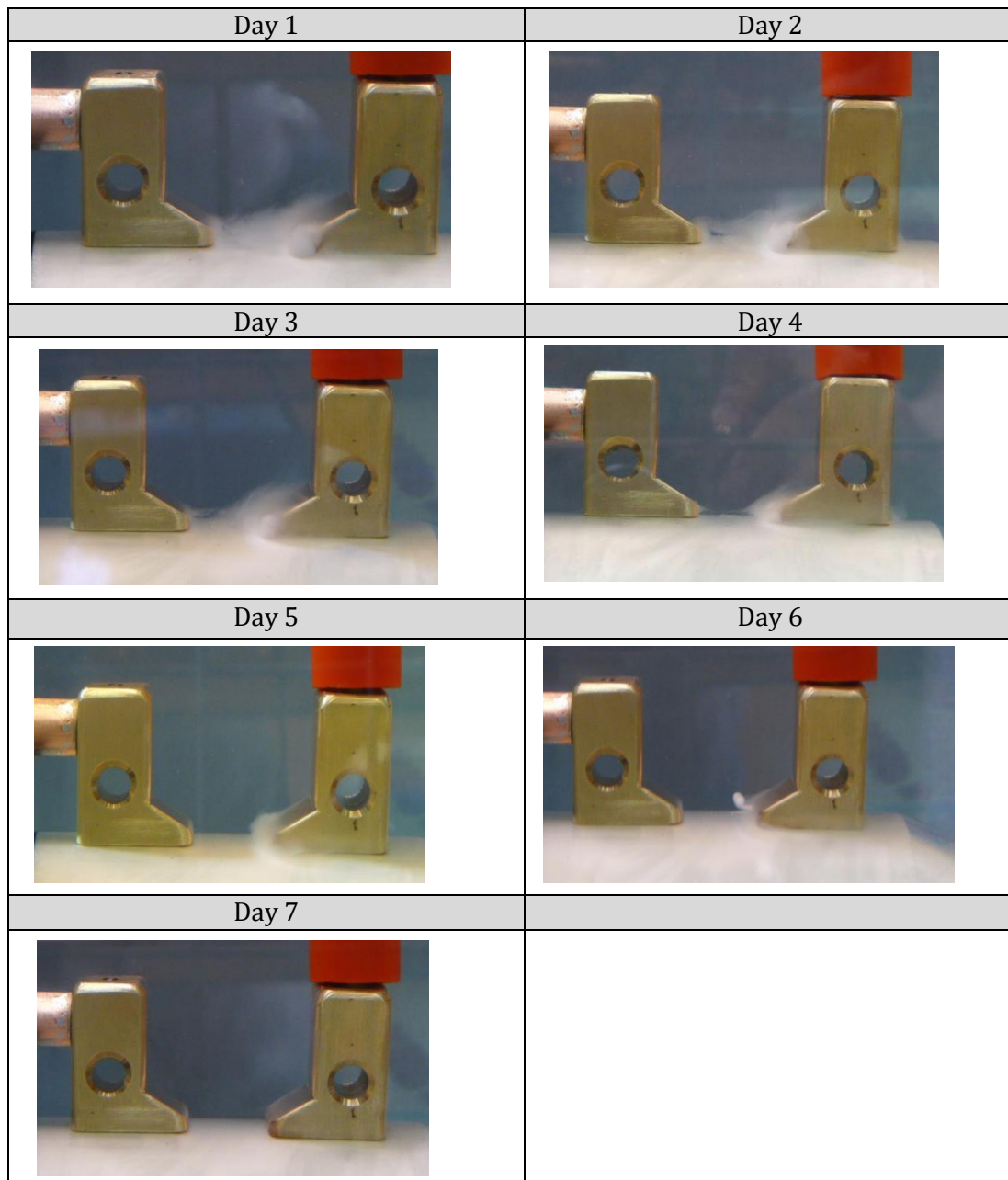
*Figure 56 The partial discharge pattern and classification map in water-oil emulsion experiments*

As in the figure above, the recorded partial discharge pattern is a mixture of surface discharge, internal discharge. In the classification map, recorded PD pattern has a relatively broad frequency spectrum, roughly from 12MHz to 23MHz. In order to know the composition of this PD signal, we dissected the resulting classification map in both the frequency domain and the time length domain. We cannot extract certain type of PD signal, such as internal PD, from the classification map by dissecting on the equivalent frequency domain. We also tried to distinguish the PD signals by dissecting on the time length domain. The results show that all types of PD spread cross the time length map.

#### 4.6. PD measurement on long term process

The experiments of water-oil emulsion on the stress cone surface gave us the information about the PD pattern. But for the company, we would also like to know the possibilities of detecting the PD signals. In other word, we would like to know the long term effect of the water-oil emulsion. In order to investigate the long term phenomenon, we did a continuous test for 7 days. The testing emulsion sample we used is 500ppm. The emulsion was injected on the stress cone surface by a syringe. After the injection, we waited until all the visible air bubbles coming out of the targeting region. The voltage was applied from 0 kV and was increased in a step of 2.5 kV/2minutes. When it reached 30 kV, the voltage stayed there for the whole week without interruption. The change in the region and the movement of the emulsion were captured by the camera and the PD signals were recorded by the Techimp PD receiver.

*Table 13 The change of the water-oil emulsion formation in 7 days*



The water oil emulsion was getting really cloudy after aging. Instead of looking like colloid, it became more white. The emulsion were coving the whole surface in between the electrodes. It seems that the cloud was dragged by the HV electrode to the right direction. The toe of the HV electrode was also covered by the emulsion. The PD signal we got is shown below.

Table 14 PD pattern results from PD measurement at different time

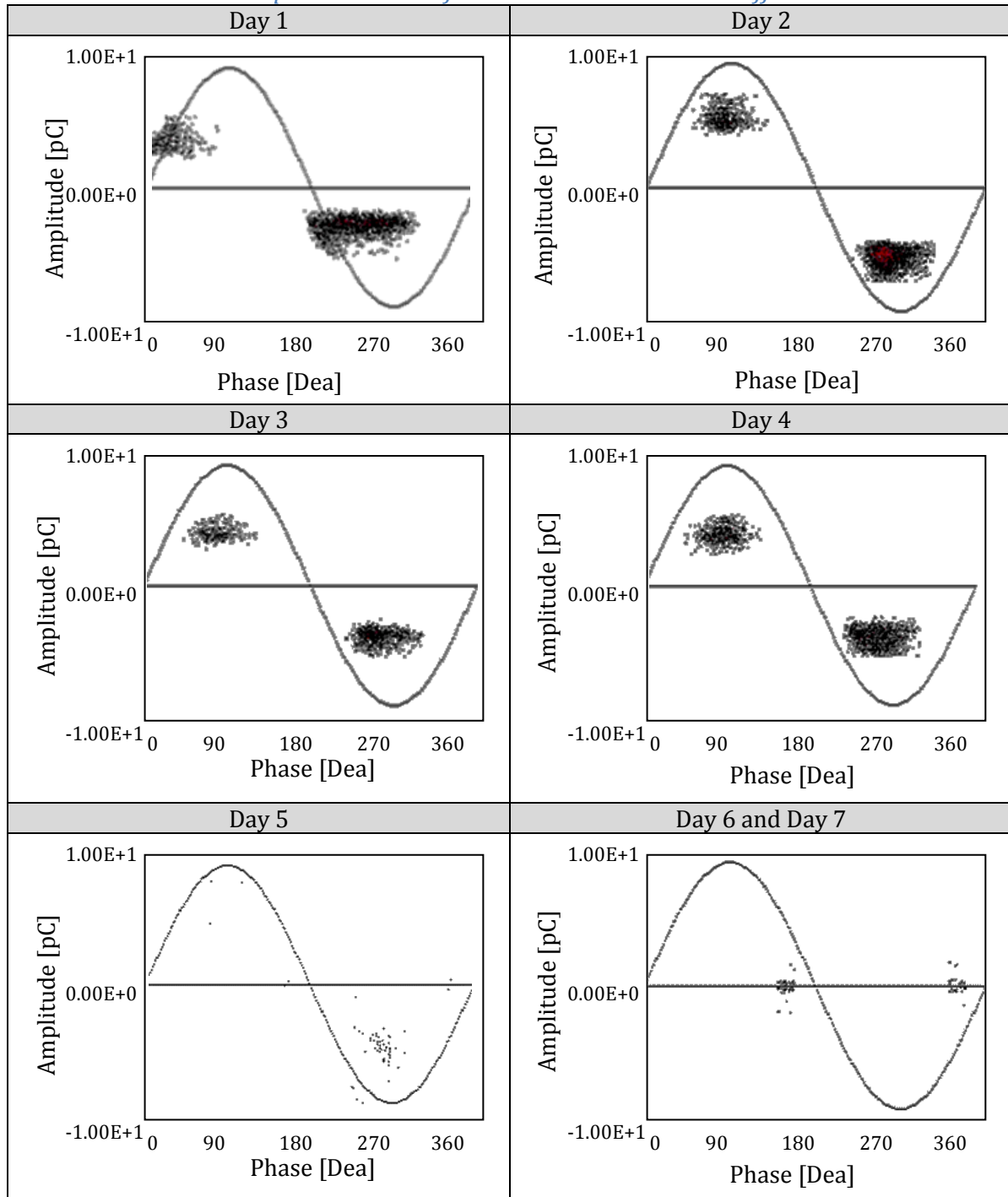
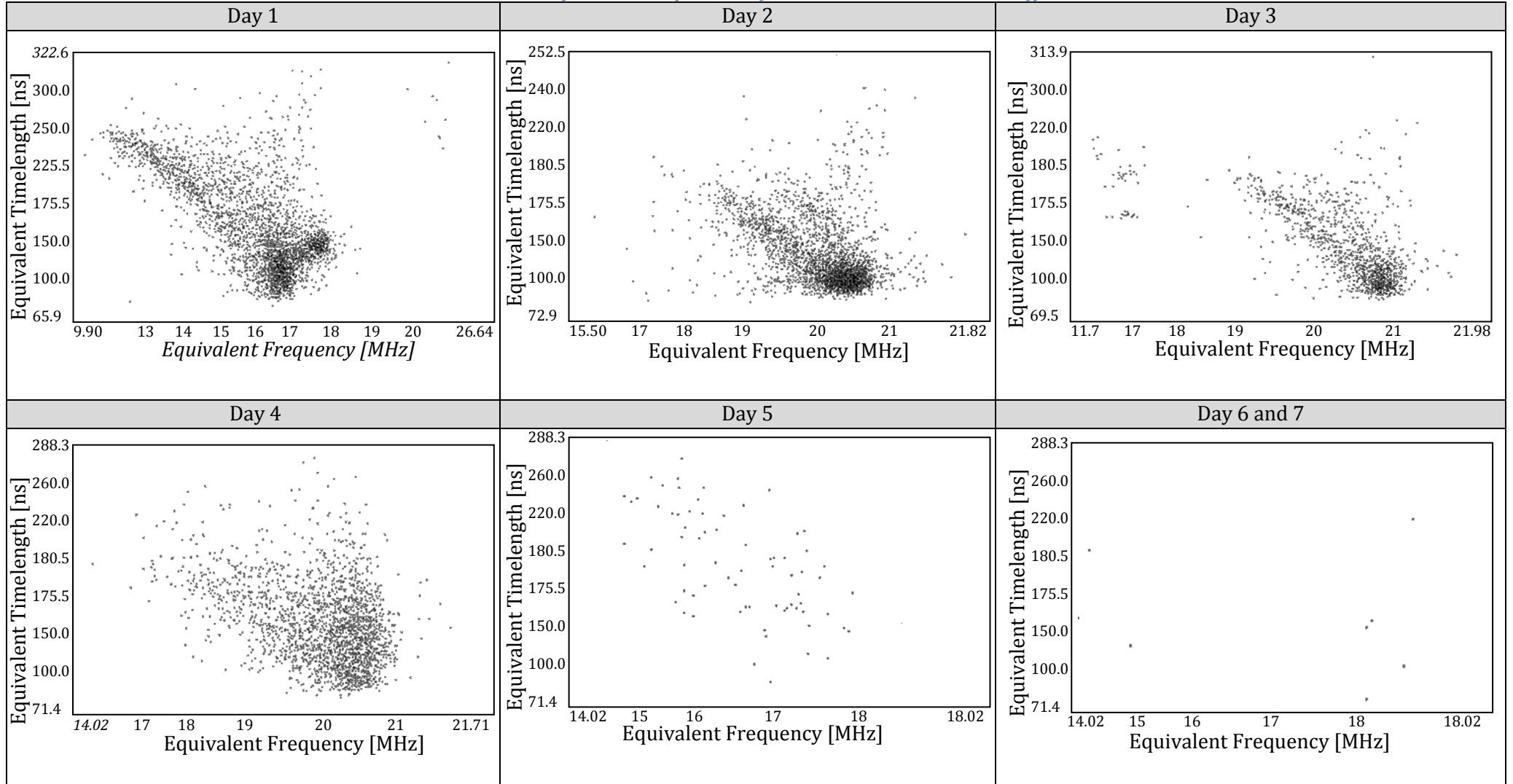


*Table 15 PD classification map results from PD measurement at different time*



The frequency spectrum is similar to the one we got in the short term test. This also has a large frequency range. On the second day of the test, the emulsion on the surface was not as bright as it was one day before. And the amount of the emulsion was decreased. A clear interface between the emulsion and the rubber surface appeared. Large amount of the emulsion gathered near the HV toe. Some of the emulsion even went behind the HV electrode. The PD signal we detected on the second day has a higher amplitude, 7pC. And the majority of the PD happened at the peak of the sinusoidal wave. It has a narrow frequency spectrum compared to the day before. On the day three, half of the water-oil emulsion was moving away from the grounding electrode. There was only a thin layer of the emulsion in between the electrodes. The emulsion is more like snow than cloud. The PD amplitude went back to 5pC and had a similar shape of the frequency spectrum. On the fourth day, there was only a little emulsion left near the grounding electrode. The bottom of the HV electrode was surrounded by the emulsion. The PD pattern and the frequency spectrum was similar to the day before. On the fifth day, there was no much emulsion on the targeting region. Only the front toe of the HV electrode were stayed with the emulsion. The PD signals were really rare. On the sixth day, even the emulsion on near the HV electrode was gone. There were some little water droplet on the cone surface and the emulsion were changing in a weird way. After seven days, there were no visible emulsion in the region anymore.

## 5 Tan $\delta$ measurement

Besides PD measurement,  $\tan\delta$  is also measured as an indication of dielectric. For an insulating material, inherent resistive losses and lossless, or capacitive, counterpart can be represented in the same complex plane. The angle between the loss component and capacitive component is called dielectric loss angle  $\delta$ . The resulting loss due to resistive component can be written as

$$W = U^2 \cdot \omega C \cdot \tan\delta \quad (18)$$

In which  $W$  is the resistive losses,  $U$  is the applied voltage,  $\omega$  is angular frequency. These are the given experimental parameters. The  $\tan\delta$  is decided by the dielectric itself. The losses increase with the increase of the  $\tan\delta$ . Therefore it can be used to evaluate the insulating performance of the dielectric. This loss can be illustrated in the equivalent circuits below. In the circuit, resistor represents the loss source.

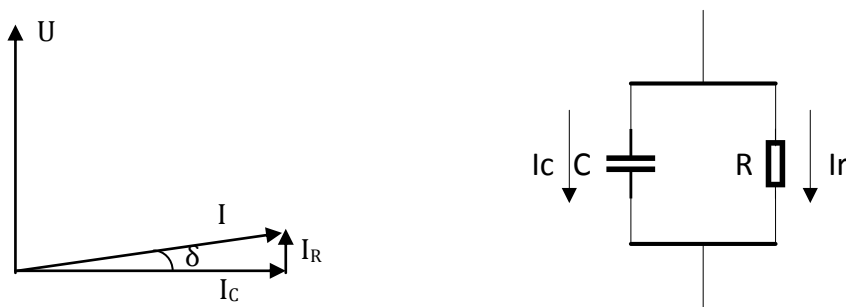


*Figure 57 Complex plane of the losses in dielectric; Parallel equivalent circuit*

In the former study [7],  $\tan\delta$  of oil-water emulsion was measured in a delicate test setup. In our research, we hope to know if it is possible to measure it on the oil-rubber interface. If the presence of water contamination can be indicated by the change of  $\tan\delta$ , then later on this technique can be developed into a handy tool for the company. Normally the  $\tan\delta$  value of high voltage equipment is below  $100 \cdot 10^{-4}$  [23].

The device we use in the  $\tan\delta$  measurement is Megger® IDAX-300 Insulation Diagnostic Analyzer. The output voltage of the device can be increased to 2 kV by using an external high voltage amplifier.



*Figure 58 tan $\delta$  measurement device and voltage amplifier*

IDAX measures the impedance of sample under certain frequency and amplitude. Later on, the parameters such as resistance, capacitance and loss can be calculated.

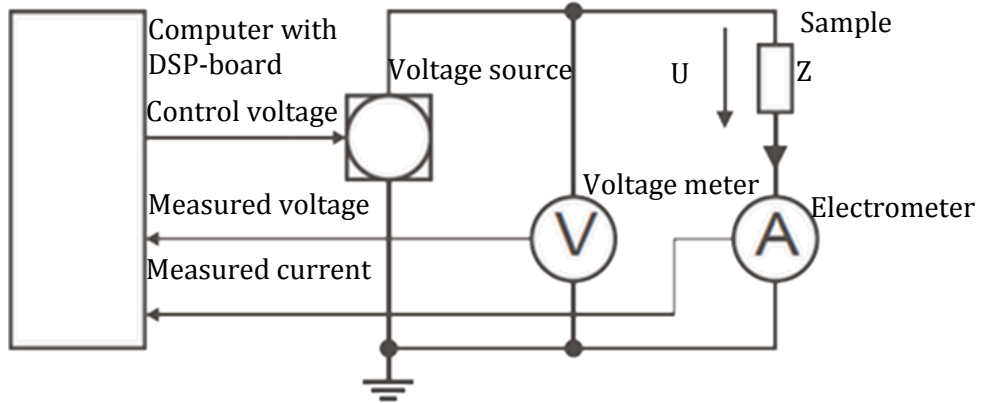


*Figure 59 The IDAX impedance measuring circuit*

The impedance is calculated by using Ohm's law,

$$Z = \frac{U}{I} \quad (19)$$

where Z, U, I are complex entities. The voltage is generated by the voltage amplifier which levels the voltage up to 2 kV. The voltage and the current are measured by the voltmeter and electrometer. The received analogue signals are then transferred into digital signals for later calculations. The  $\tan\delta$  can be derived from

$$\tan\delta = -\frac{\text{Re}\{Z\}}{\text{Im}\{Z\}} \quad (20)$$

This digital way of getting  $\tan\delta$  is more convenient than the traditional Schering bridge method. The circuit for measuring the  $\tan\delta$  is based on the given configuration. Since it is not easy to get rid of the coupling capacitor in our test setup, we choose to use the configuration below. The capacitor CR is the our test setup in between the detecting lead.

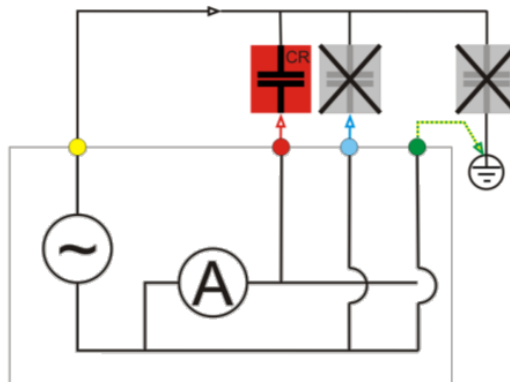
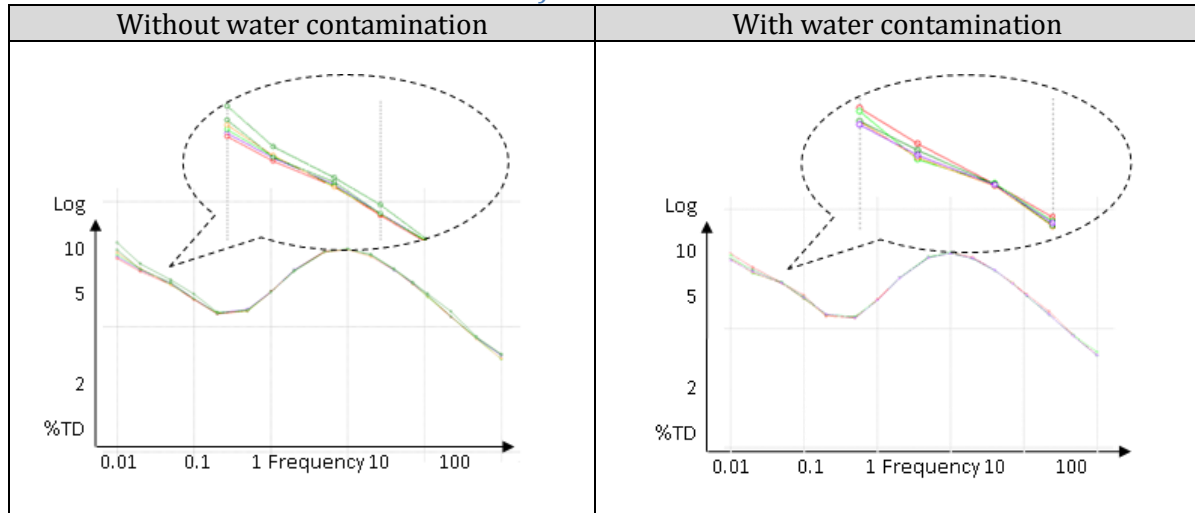


*Figure 60 Measuring circuit for the tan  $\delta$*

*Table 16 tan $\delta$  on the stress cone surface with and without water contamination*



First we measured the tan $\delta$  of the oil without water contamination, under different voltage levels. The electrodes distance was 2.5cm, and the applied voltages were 140V, 250V, 500V, 750V, 1000V, 1250V. The measuring frequency ranges from 0.01Hz to 1kHz. From the result we can see that the tan $\delta$  value does not change much with the applied voltages. But the tan $\delta$  value is very high considering the quality of the oil. After that, we injected water emulsion with 700ppm. We set it with the same measuring voltages and frequencies. The resulting values show the same trends and values compared with previous experiment. Since the measured tan $\delta$  is relatively high, this similarity cannot be caused by the detection limit of the IDAX. Considering the complex configuration of our test setup, we believe the fixation metal was not properly isolated from the ground. So the leakage current was added by the current went through the fixation metal to grounding lead. In order to isolate the test subject from the fixation metal, we put a Teflon ring between the conducting bar and the fixation metal.

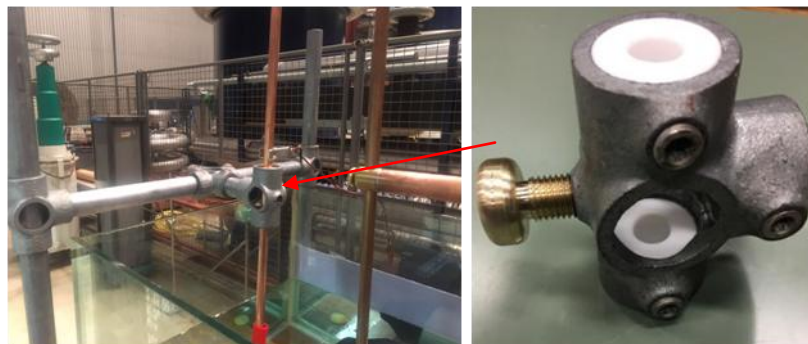


*Figure 61 Teflon ring for isolating the conducting bar and grounding lead*

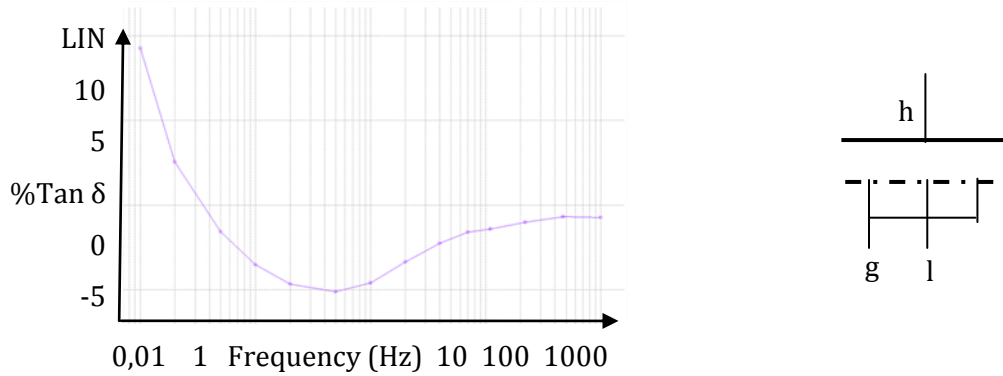


*Figure 62  $\tan \delta$  on stress cone with water contamination after putting Teflon ring; three terminal circuit*

After putting the Teflon ring, we measured the  $\tan \delta$  with water contamination again. The measurement was done at 200V, under variant frequency. The measured  $\tan \delta$  is shown above. It is beyond question that the value of the  $\tan \delta$  cannot be negative, since it indicates the losses in the insulating material. However the three terminal circuit in the measuring system, such as in the standard capacitor, may results in a negative result especially when the loss in the setup is very low [48]. Considering the large size of the detecting area, and complexity of our configuration there is also a big chance to have noise intrusion in the measuring process. The formidable insulating property of the oil results a relatively small leakage current. So the desired signal might be overlapped by the noise in the setup.

In order to amplify the influence brought by the water contamination and measure the leakage current precisely, we need to scale down our test setup.

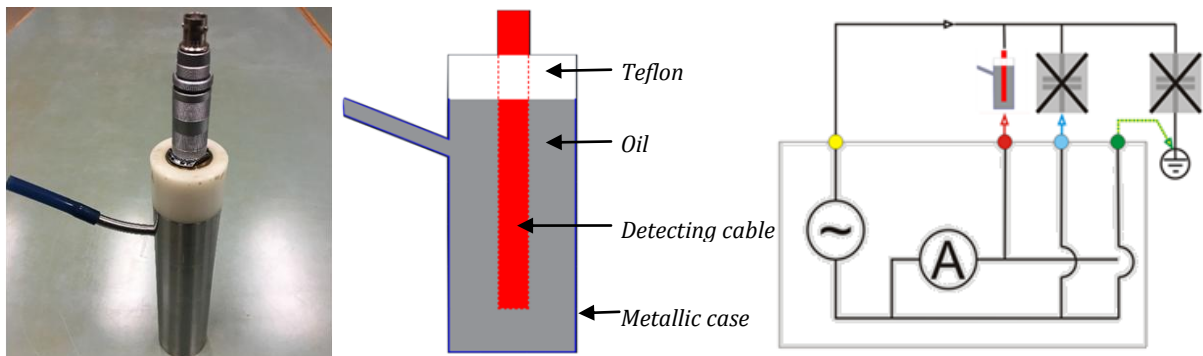


*Figure 63 Dedicated  $\tan \delta$  measuring device and detecting circuit*

The measuring device we used is invented by TU Delft. This kettle-like equipment is dedicated to precisely measure the  $\tan \delta$  value of the liquid. As we can see from the figure above, the liquid needs to be measured is injected in the space between the detecting cable and metallic case. The detecting cable is connected with the voltage source and the metallic case is connected with the leakage current meter. We measured the  $\tan \delta$  of both the clean oil and water-oil emulsion at 700ppm. The measurements were done at 200V, under variant frequency. The results are presented below: the top curve is the  $\tan \delta$  of the emulsion and the bottom one is for clean oil.

The  $\tan \delta$  of both samples decreases with the increasing of the frequency. But  $\tan \delta$  of water-oil emulsion is much more higher than the  $\tan \delta$  of clean oil. This indicates that, under a well-defined

testing environment,  $\tan\delta$  can be used to detect the presence of water contamination. But due to the complexity of a real onsite termination, this measuring technique can hardly be adopted.

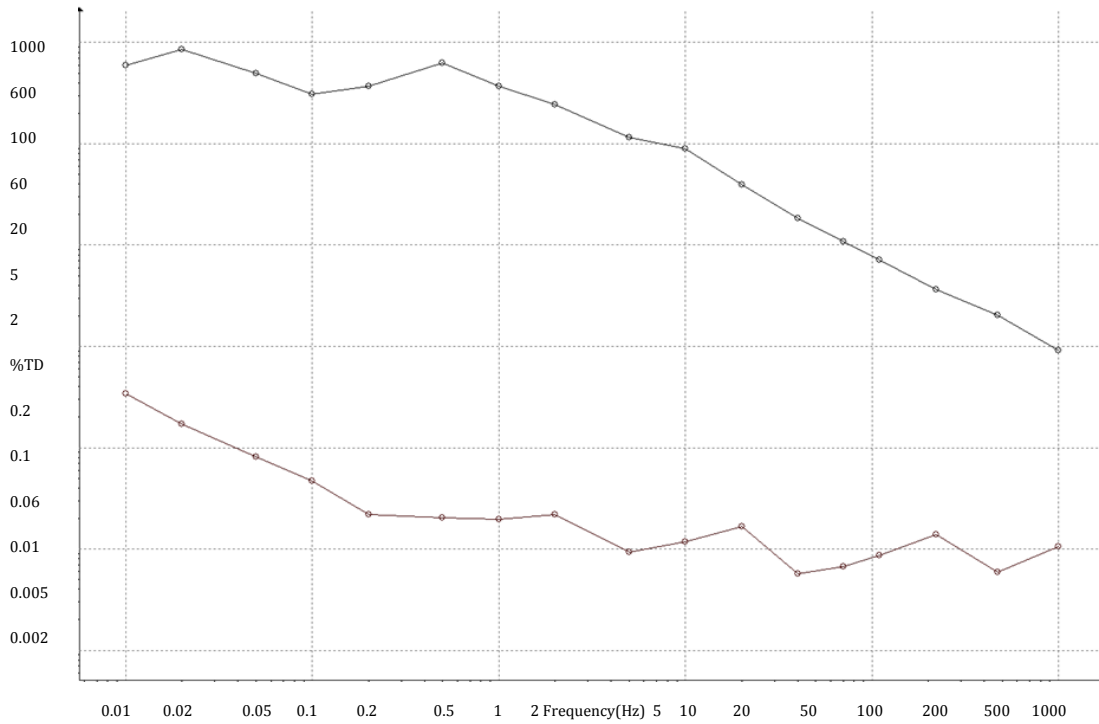


Figure 64  $\tan\delta$  of pure oil(line below) and water-oil emulsion(line above)

# 6 Conclusions & Recommendations

## 6.1. Conclusions

Based on the simulation results and experiments observations, we can make conclusions as follow:

### ➤ **Electric field distributions on the stress cone surface with water contamination**

Water content tends to move along the opposite direction of the electric field. Electric field direction on the stress cone surface has two compositing components. One is from inner cable to the cone outside, and the other one is from top to bottom. The first direction component attracts water to the stress cone surface. The electric field along the interface apply force on the water content and deforms water into smaller particles. On the other hand, water contamination also affects electric field distribution. Main parameters that affect the electric field includes the positions of the water droplets, size of the droplets, relative permittivity of water contamination and the number or covering area of the water contamination.

### ➤ **Water content detecting by PD measurement**

Based on our measurement results, PD activities due to water contamination on the stress cone surface is a mixture signals of surface discharges and internal discharges. The PD pattern and classification map are recognized. These information can be used as an indication for onsite moisture detection. However, based on our observation, the occurrence of the PD signals is not constant. This implies that in order to get the PD signal, terminations have to be monitored in at least certain amount of time. The recommendation for the measurement period is 2 hours.

### ➤ **Water content detecting by $\tan \delta$ measurement**

In our delicate test setup, the  $\tan \delta$  of the termination oil can be increased by several orders due to the presence of water contamination. However, in our small scale test setup, the change of the  $\tan \delta$  value cannot be detected when there is water-oil emulsion on the oil-rubber interface. Considering the bulky size and complex content in a real termination, water contamination detecting by  $\tan \delta$  measurement is even more unpromising.

## 6.2. Recommendations

Taking into account the potential academic contributions and the needs from the company, we also have three pieces of recommendations for future work.

### ➤ **Test setup design on long term experiment**

As we can see from the 7 days experiment on our test setup, the water-oil emulsion kept moving away from the electrodes. This should be taken into account when designing test setup to investigate the aging phenomenon on the stress cone surface due to water contamination.

### ➤ **Investigations on triple points in the oil termination**

The importance of the interface is already strongly addressed in this thesis work. Besides the interface, triple points in a real termination is also highly worth of investigating since the degradation often starts from there. Due to a limited amount of time given for our thesis work, the research on triple points cannot be deployed. The 3D model used in the simulations can also be used with an intention on triple points such as the transition at the end of the stress cone or the junction formed by oil, water and rubber.

### ➤ **PD sensor design and installations**

Even though the PD pattern and its frequency range are already recognized, practical solutions for the design and installation of PD sensors for oil terminations still need to be discussed. This requires to think about the reliability of the sensor, the convenience the installation and the cost-effectiveness for manufacturing.

### ➤ **Development of non-electrical detections**

Besides PD and  $\tan\delta$  measurements, non-electrical detecting methods should also be discussed in future works. As mentioned in this report, water contamination may cause regional temperature increasing in oil terminations, thus an infrared thermal meter could be used for detecting. A moisture sensor based on fluid motions can also be tested for the type of oil in the termination. In the end, it might be necessary to implement a combination of different sensors to get convincing detecting results.

## Reference

- [1] [http://www.yacht-chartercroatia.com/about\\_croatia/tesla/tesla-ac-system.htm](http://www.yacht-chartercroatia.com/about_croatia/tesla/tesla-ac-system.htm)
- [2] F. H. Kreuger, *Industrial High Voltage - Volume I*, Delft: Delft University Press, 1991.
- [3] Mauseth, Frank, Sverre Hvidsten, and Geir Birkenes. "Surface degradation of XLPE insulation at oil-water interfaces." *Electrical Insulation and Dielectric Phenomena (CEIDP), 2011 Annual Report Conference on*. IEEE, 2011.
- [4] Liland, Knut Brede, et al. "Failure Modes and Condition Assessment of High Voltage Oil Filled XLPE Terminations." *29th Electrical Insulation Conference Montreal, CANADA, MAY31-JUN03*. 2009.
- [5] Liland, K. B., et al. "Measurement of solubility and water content of insulating oils for HV XLPE Cable Terminations." *Electrical Insulation, 2008. ISEI 2008. Conference Record of the 2008 IEEE International Symposium on*. IEEE, 2008.
- [6] Chengwei, Chen, et al. "The study on evaluation model for water in silicone oil of cable termination and simulate experiment." *Electrical Insulation, 2008. ISEI 2008. Conference Record of the 2008 IEEE International Symposium on*. IEEE, 2008.
- [7] J. weiwen. "Condition assessment of water in high viscosity cable termination oil." MSc thesis. 2016.
- [8] Nelson, J. Keith. "Motion at the liquid-solid interface-developing design tools from fundamental models." *Dielectric Liquids, 2002. ICDL 2002. Proceedings of 2002 IEEE 14th International Conference on*. IEEE, 2002.
- [9] Argirakis, I., et al. "The liquid-solid interface: the effect of negative liquid discharge." *Dielectric Materials, Measurements and Applications, Seventh International Conference on (Conf. Publ. No. 430)*. IET, 1996.
- [10] Weinan, Fan, et al. "Study on diagnostic method of aging 10 kV XLPE cable." *Electricity Distribution (CICED), 2016 China International Conference on*. IEEE, 2016.
- [11] Liang, Zipeng, et al. "Aging state assessment of 110 kV XLPE cable based on IRC and AE." *Power and Energy Engineering Conference (APPEEC), 2016 IEEE PES Asia-Pacific*. IEEE, 2016.
- [12] Lothongkam, Chaiyaporn, et al. "The influence of thermal aging on AC dielectric strength of transparent silicone rubbers for HV insulation." *Electrical Insulating Materials (ISEIM), Proceedings of 2014 International Symposium on*. IEEE, 2014.
- [13] Wechsler, Kenneth, and Michael Riccitiello. "Electric breakdown of a parallel solid and liquid dielectric system." *Transactions of the American Institute of Electrical Engineers. Part III: Power Apparatus and Systems* 80.3 (1961): 365-368.
- [14] Kelley, E. F., and R. E. Hebner. "Electrical breakdown in composite insulating systems: liquid-solid interface parallel to the field." *IEEE Transactions on Electrical Insulation* 4 (1981): 297-303.
- [15] Mohamed, EL-Adawy, et al. "Physicochemical analysis at the interface between conductive solid and dielectric liquid for flow electrification phenomenon." *IEEE Transactions on Industry Applications* 46.4 (2010): 1593-1600.
- [16] Chatterjee, S., et al. "Electric field computation in presence of water droplets on a polymeric insulating surface." *Control, Instrumentation, Energy & Communication (CIEC), 2016 2nd International Conference on*. IEEE, 2016.

- [17] Nazemi, M. H., and V. Hinrichsen. "Experimental investigations on water droplet oscillation and partial discharge inception voltage on polymeric insulating surfaces under the influence of AC electric field stress." *IEEE Transactions on Dielectrics and Electrical Insulation* 20.2 (2013): 443-453.
- [18] Panagiotis Tsakonas. "Design and development of a 72 kV cable Y-joint with integrated PD sensor for offshore wind turbine grid connections." MSc thesis. 2016.
- [19] Worfolk, Brian J., et al. "Ultra-high electrical conductivity in solution-sheared polymeric transparent films." *Proceedings of the National Academy of Sciences* 112.46 (2015): 14138-14143.
- [20] Patel, Utkarsh, Shesha H. Jayaram, and Ayman El-Hag. "Analysis of cable termination under power frequency and high frequency voltages." *Electrical Insulation and Dielectric Phenomena (CEIDP), 2011 Annual Report Conference on. IEEE, 2011.*
- [21] L. Simoni, *Fundamentals of endurance of electrical insulating materials*, CLUEB, Bologna, Italy, 1st issue 1983, 2nd issue 1994.
- [22] T.W. Dakin, "The endurance of electrical insulation", *Proc. 4th Symp. Elec. Insul. Materials, IIEE*, September 1971.
- [23] T. Tanaka, A. Greenwood, *Advanced Power Cable Technology*, Vol. 1, CRC Press, Boca Raton, USA, 1983.
- [24] G.C. Montanari, "Aging and life models for insulation systems based on PD detection", *IEEE Trans. Diel. El. Insul.*, Vol. 2, No. 4, pp. 667-675, 1995.
- [25] Kreuger, Frederik H. "Industrial High Voltage: 4. Coordinating, 5. Testing, 6. Measuring." (1992).
- [26] Al-Masri, Wasim MF, Mamoun F. Abdel-Hafez, and Ayman El-Hag. "A multi-hypothesis sequential probability test for partial discharges localization in power transformers." *Mechatronics and its Applications (ISMA), 2015 10th International Symposium on. IEEE, 2015.*
- [27] Fuangsoongnern, Urairat, Winai Plueksawan, and Kittimasak Tikakosol. "A measurement technique to identify and locate partial discharge in transformer with AE and HFCT." *Innovative Smart Grid Technologies-Asia (ISGT Asia), 2014 IEEE. IEEE, 2014.*
- [28] Bologna, Fabio Franco, J. P. Reynders, and A. C. Britten. "Corona discharge activity on a string of glass cap-and-pin insulators under conditions of light wetting, light non-uniform contamination." *Power Tech Conference Proceedings, 2003 IEEE Bologna. Vol. 3. IEEE, 2003.*
- [29] Boggs, S. A., and G. C. Stone. "Fundamental limitations in the measurement of corona and partial discharge." *IEEE Transactions on Electrical Insulation* 2 (1982): 143-150.
- [30] Jahoda, Emil, et al. "Study of the surface discharge on the air-insulation interface." *ELEKTRO, 2016. IEEE, 2016.*
- [31] Suhaimi, N. S., et al. "Investigation on breakdown strength of mineral oil based carbon nanotube." *Power and Energy (PECon), 2016 IEEE International Conference on. IEEE, 2016.*
- [32] Kelley, E. F., and R. E. Hebner. "Electrical breakdown in composite insulating systems: liquid-solid interface parallel to the field." *IEEE Transactions on Electrical Insulation* 4 (1981): 297-303.
- [33] Danikas, Michalis G., and Alan J. Pearmain. "Study of movement and stability of an injected air bubble in a uniaxially oriented polyethylene/oil insulation system under electric stress." *Electrical Insulation, 1984 IEEE International Conference on. IEEE, 1984.*
- [34] Kaatz, Udo. "Complex permittivity of water as a function of frequency and temperature." *Journal of Chemical and Engineering Data* 34.4 (1989): 371-374.
- [35] Geert R. Langereis, Wouter Olthuis\* and Piet Bergveld. "Tap water hardness estimated by conductivity measurement to reduce detergent dosing" Unpublished
- [36] Berg, Gunnar, et al. "Instability of electrically stressed water droplets in oil." *Dielectric Liquids, 2002. ICDL 2002. Proceedings of 2002 IEEE 14th International Conference on. IEEE, 2002.*

- [37] Taylor, Geoffrey. "Disintegration of water drops in an electric field." Proceedings of the Royal Society of London A: Mathematical, Physical and Engineering Sciences. Vol. 280. No. 1382. The Royal Society, 1964.
- [38] Tsabek, L. K., G. M. Panchenkov, and V. V. Papko. "Theoretical basis of operation of equipment for electrical dehydration and electrical desalting of oil emulsions." 8th World Petroleum Congress. World Petroleum Congress, 1971.
- [39] Florence, A. T., and D. Whitehill. "Some features of breakdown in water-in-oil-in-water multiple emulsions." Journal of Colloid and Interface Science 79.1 (1981): 243-256.
- [40] Kreuger, F. H., E. Gulski, and A. Krivda. "Classification of partial discharges." IEEE transactions on Electrical Insulation 28.6 (1993): 917-931.
- [41] Midmore, B. R. "Preparation of a novel silica-stabilized oil/water emulsion." Colloids and Surfaces A: Physicochemical and Engineering Aspects 132.2-3 (1998): 257-265.
- [42] Abismail, B., et al. "Emulsification by ultrasound: drop size distribution and stability." Ultrasonics Sonochemistry 6.1 (1999): 75-83.
- [43] Ansmann, Achim, et al. "Oil-water emulsifiers." U.S. Patent No. 6,264,961. 24 Jul. 2001.
- [44] Abu-Zaid, M. "Performance of single cylinder, direct injection diesel engine using water fuel emulsions." Energy Conversion and Management 45.5 (2004): 697-705.
- [45] Wikipedia Parts per million: [https://nl.wikipedia.org/wiki/Parts\\_per\\_million](https://nl.wikipedia.org/wiki/Parts_per_million)
- [46] Gold, P. W., et al. "Viscosity-pressure-temperature behaviour of mineral and synthetic oils." Lubrication Science 18.1 (2001): 51-79.
- [47] Chen, Gonglun, and Daniel Tao. "An experimental study of stability of oil-water emulsion." Fuel processing technology 86.5 (2005): 499-508.
- [48] Yao-nan, Liu, and Liu Chyi-Chang. "The study of apparent negative value in measuring dielectric loss." IEEE Transactions on Electrical Insulation 1 (1982): 20-26.